

Temporal signatures of lepto-hadronic feedback mechanisms in compact sources

M. Petropoulou ^{*} and A. Mastichiadis [†]

Department of Physics, University of Athens, Panepistimiopolis, GR 15783 Zografos, Greece

Received.../Accepted...

ABSTRACT

The hadronic model of Active Galactic Nuclei and other compact high energy astrophysical sources assumes that ultra-relativistic protons, electron-positron pairs and photons interact via various hadronic and electromagnetic processes inside a magnetized volume, producing the multiwavelength spectra observed from these sources. A less studied property of such systems is that they can exhibit a variety of temporal behaviours due to the operation of different feedback mechanisms. We investigate the effects of one possible feedback loop, where γ -rays produced by photopion processes are being quenched whenever their compactness increases above a critical level. This causes a spontaneous creation of soft photons in the system that result in further proton cooling and more production of γ -rays, thus making the loop operate. We perform an analytical study of a simplified set of equations describing the system, in order to investigate the connection of its temporal behaviour with key physical parameters. We also perform numerical integration of the full set of kinetic equations verifying not only our analytical results but also those of previous numerical studies. We find that once the system becomes ‘supercritical’, it can exhibit either a periodic behaviour or a damped oscillatory one leading to a steady state. We briefly point out possible implications of such a supercriticality on the parameter values used in Active Galactic Nuclei spectral modelling, through an indicative fitting of the VHE emission of blazar 3C 279.

Key words: astroparticle physics – radiation mechanisms: non-thermal – gamma rays: galaxies – galaxies: active

1 INTRODUCTION

The idea that high energy protons can be produced in Active Galactic Nuclei (AGN) has been suggested by Kazanas & Ellison (1986) who considered proton acceleration by shock waves in the inner regions of these objects. Following on this idea, Sikora et al. (1987) suggested that, in this case, relativistic protons will lose energy in photohadronic interactions with the abundant soft photons rather than via inelastic collisions with the ambient cold protons. These ideas were later applied to the blazar jets (Mannheim 1993; Mücke & Protheroe 2001) giving rise to what is known today as the hadronic model for blazar high energy emission – for a review see Böttcher (2007) and Böttcher (2010). Similar ideas have been applied also to Gamma Ray Bursts (Böttcher & Dermer 1998, Kazanas, Georganopoulos, & Mastichiadis 2002, Mastichiadis & Kazanas 2006; Asano & Inoue 2007; Asano, Inoue, & Mészáros 2009; Mastichiadis &

Kazanas 2009) and γ -ray emitting compact binary systems¹ (Romero et al. 2003; Paredes, Bosch-Ramon, & Romero 2005; Romero, Christiansen, & Orellana 2005) in order to explain the high energy emission from these objects. The hadronic models therefore form a viable alternative to the commonly used leptonic ones.

High energy protons will radiate by synchrotron radiation, as well as by photopair and photopion while interacting on any soft photon present. These interactions will produce secondaries: electron/positron pairs which are produced directly from photopair and via charged pion decay from photopion interactions as well as gamma-rays via neutral pion decay again from photopion; there will be also neutrino and neutron production coming as byproducts of photopion. While neutrinos will escape the source without

¹ There is a difference between hadronic models describing such systems and the corresponding ones used in modelling AGN or GRB high energy emission. The physical conditions in compact binary systems favour inelastic pp -collisions instead of photohadronic interactions, which for this reason are neglected.

^{*} E-mail: maroulaaki@gmail.com

[†] E-mail: amastich@phys.uoa.gr

any interactions and so their spectrum will be that at production, the created electron/positron pairs will lose energy through synchrotron radiation and inverse Compton scattering while gamma-rays will be absorbed in photon-photon collisions. Therefore in order to calculate the emerging photon spectrum one has to follow the evolution of these secondaries which can be complicated due to the formation of intense electromagnetic (EM) cascades initiated, e.g., by γ -rays from π^0 decay.

Usually the modelling of hadronic processes assumes that the target photons come either from an external source or from synchrotron radiation of a co-accelerated leptonic component. One largely overlooked aspect is the possibility that protons interact with their own radiation, for example, with the soft photons produced from the aforementioned EM cascades. First attempts to incorporate these into the models were made by Stern & Svensson (1991) and Stern, Sikora, & Svensson (1992). Using Monte Carlo simulations the above authors found that the system of protons and photons can exhibit limit cycles. However, this oscillating behaviour of the system could not be interpreted as the result of a specific feedback mechanism, let alone studied in a systematic way. One of the operating feedback processes was studied analytically by Kirk & Mastichiadis (1992) using the kinetic equation approach². They showed that a sufficient number density of protons can make the system unstable, causing runaway pair production: synchrotron photons of the relativistic electron-positron pairs become targets for the protons which produce more pairs. The feedback leads eventually to fast proton energy losses. This amount of energy lost by the protons in a small time interval is transferred to photons and it is seen as a flaring event. The operation of this feedback loop was later confirmed numerically by Mastichiadis & Kirk (1995) and Mastichiadis, Protheroe, & Kirk (2005), who also found cases where the system showed a limit cycle behaviour.

In the present paper we examine another type of feedback which can operate in hadronic systems. For this we capitalize on the ideas of non-linear photon quenching (Stawarz & Kirk 2007; Petropoulou & Mastichiadis 2011). According to this, γ -rays produced in a spherical volume cannot exceed a critical luminosity that depends only on the source's magnetic field and radius. If they do, then soft photons will be produced automatically and quench the 'excessive' γ -rays. In the context of a hadronic system γ -rays can either be produced directly by proton synchrotron radiation or indirectly by photopair and photopion interactions. Then the following loop suggests itself:

(i) Protons cool on soft photons producing γ -rays.

(ii) The γ -ray luminosity is quenched and turned spontaneously into soft photons which feedback on 1.

Clearly this mechanism can tap energy stored in protons and transfer it to radiation. At the same time it shows that the hadronic system is a dynamical one and its behaviour can be more complex than it is customarily assumed. A detailed study of the aforementioned feedback mechanism, in

the case where γ -rays are the byproduct of photopion interactions, will be the subject of the present work. The paper is structured as follows: In §2 we describe qualitatively the system and define two regimes of operation. Next we construct a system of non-linear equations which we solve first analytically in a simplified form (§3). In §4 we show in a semi-analytical way the role of various processes on the dynamical behaviour of the system, while in §5 we back our results presenting a full numerical study of the problem. In §6 we present an indicative astrophysical example, where some of our results are applied to the blazar 3C 279. Finally, we conclude in §7 with a summary and discussion.

2 QUALITATIVE DESCRIPTION OF THE PHYSICAL SYSTEM

2.1 Linear regime

We assume a spherical source of radius R with embedded magnetic field B and a monoenergetic proton distribution of number density \tilde{n}_p and Lorentz factor γ_p . This region is also filled with monoenergetic radiation of energy ϵ_o (normalized to electron rest mass energy) and number density \tilde{n}_{ex}^3 , which we will assume comes from outside of the source. Thus, we denote it as 'external'.

The injected high energy protons will interact with the external photons through inelastic photopair and photopion collisions, provided that the respective threshold conditions are satisfied. We will assume that the condition

$$\epsilon_o \gamma_p \gtrsim \frac{m_\pi}{m_e}, \quad (1)$$

where m_π is the pion mass, is always satisfied. This means that both photopair and photopion operate; however since the target photons are monoenergetic, it guarantees that photopion will be the main loss mechanism for protons (Sikora et al. 1987; Begelman, Rudak, & Sikora 1990). The produced charged and neutral pions will decay producing electron/positron pairs (for brevity we will refer to them simply as 'electrons') and γ -rays. The former will radiate photons mainly through the synchrotron process, since inverse Compton scattering will be greatly suppressed by Klein-Nishina effects. We will refer to these synchrotron photons as 'hard', since for proton energies with values typical of the AGN hadronic models, these can in principle emerge in the γ -ray regime.

One can quantify the above by noting that the secondary electrons from the charged pion decay are produced with a Lorentz factor

$$\gamma_{e,\pi} \approx \eta_p \gamma_p \frac{m_p}{m_e}, \quad (2)$$

where $\eta_p = k_p/4 \simeq 0.08$ and k_p is the inelasticity of the interaction assumed to be $\simeq 0.3$. The factor $1/4$ arises from the assumed energy equipartition between the lepton and the three neutrinos produced by the charged pion decay – see Dimitrakoudis et al. (to appear in 2012). Assuming that these electrons emit at the critical synchrotron energy

$$\epsilon_h = b \gamma_{e,\pi}^2, \quad (3)$$

² A discussion about the different numerical approaches employed is presented in Stern et al. (1995).

³ We note that here and through the present work tilted quantities denote quantities with dimensions.

where $b = B/B_{cr}$ and $B_{cr} = 4.413 \times 10^{13}$ G the critical value of the magnetic field strength, we find that for typical values of $\gamma_p = 10^8$ and $B = 1$ G, ϵ_h is in the TeV regime.

Let \dot{E}_{tot} be the energy loss rate of all protons of energy γ_p due to interactions with the photons. This energy is distributed to the produced secondaries. Assuming that their cooling is fast – an assumption which is reasonable since both B and γ_e are assumed to have high values, one can argue that the energy injected into secondary electrons will be instantaneously radiated as hard photons. Then we can define the injected hard photon compactness as

$$\ell_h^{inj} = \xi_\pi \frac{\dot{E}_{tot} \sigma_T}{4\pi R m_e c^3}, \quad (4)$$

where σ_T is the Thomson cross section and ξ_π is the fraction of energy that goes to the secondary electrons. Furthermore, we can connect \dot{E}_{tot} to the single proton energy loss rate \dot{E}_p through the relation

$$\dot{E}_{tot} = \tilde{n}_p V \dot{E}_p, \quad (5)$$

where V is the volume of the source. Since photohadronic losses can be considered catastrophic, i.e., a relativistic proton can lose a substantial amount of its energy in one collision with a photon, we can write

$$\dot{E}_p \simeq k_p \tilde{E}_p c \int dx \tilde{\sigma}_{p\gamma}(\gamma_p x) \tilde{n}_{ph}(x), \quad (6)$$

where $\tilde{E}_p = \gamma_p m_p c^2$ is the proton energy, $\tilde{\sigma}_{p\gamma}$ is the relevant cross section, \tilde{n}_{ph} is the target photon population and x the target photon energy in units of $m_e c^2$. Under our assumptions, i.e., catastrophic energy proton losses and monoenergetic particle distributions, we can adopt working, from this point on, with $k_p = 1$ without loss of generality. Furthermore, we can approximate the cross section with a Heaviside function of the form

$$\tilde{\sigma}_{p\gamma}(\gamma_p, x) \simeq \sigma_{p\gamma}^0 \sigma_T H(\gamma_p x - m_\pi/m_e) \quad (7)$$

with $\sigma_{p\gamma}^0 = 10^{-4}$; for a plot of the total expression of the cross section see Fig. 3 in Mücke et al. (2000). Using also the fact that the only target photons present are the external ones, eq.(6) becomes

$$\dot{E}_p \simeq \gamma_p m_p c^2 \sigma_{p\gamma}^0 \tilde{n}_{ex}. \quad (8)$$

Combining relations (4) - (8) one can immediately deduce that the compactness (or luminosity) of the hard photons depends on both \tilde{n}_p and \tilde{n}_{ex} . In this case the system can be considered to operate in the linear regime, since all cooling is provided by the external photons.

2.2 Non-linear regime

The previous results indicate that for sufficiently high values of \tilde{n}_p or \tilde{n}_{ex} , the injected hard photon compactness can take high values as well. However, as it was shown in Stawarz & Kirk (2007) and Petropoulou & Mastichiadis (2011) – henceforth SK07 and PM11 respectively, if the hard photon compactness is larger than some critical value ℓ_h^{cr} that depends only on ϵ_h and on source parameters such as B and R , even small initial perturbations of low energy photons present in the source, can grow and lead to an automatic

quenching of the hard photons. This is a purely non-linear process. In this case, electron-positron pairs grow spontaneously in the source and the ‘excessive’ hard radiation is absorbed by the synchrotron photons emitted by the pairs. Thus, a soft photon population of number density \tilde{n}_s and energy ϵ_s appears spontaneously in the source. Assuming equipartition of energy between the created pairs one finds that ϵ_s is given by

$$\epsilon_s = b \gamma_e^2 = b \left(\frac{\epsilon_h}{2} \right)^2. \quad (9)$$

These automatically produced photons have the same energy with those produced by the absorption of hard photons on the external ones; note that this is a linear process. Thus, both linear and non-linear absorption of hard photons result in the formation of a third photon population in the system with compactness ℓ_s . This new component will start playing a role in proton cooling through eq. (6), since now $\tilde{n}_{ph} = \tilde{n}_{ex} + \tilde{n}_s$. If its number density grows sufficiently high, then it is possible that the relativistic protons will start cooling more efficiently on them than on the external photons. In this case, proton cooling becomes non-linear.

Figure 1 summarizes the different processes operating in the system. Arrows leading to the circles of Fig. 1 denote injection of the corresponding particle species into the source, whereas arrows coming out of the circle of hard photons imply their subsequent absorption. In order to emphasize the existence of two absorbing channels for the γ -rays, the non-linear one is shown with a dashed line. We note also that the secondary electrons that are the intermediate products of the different processes operating in the system and responsible for the emission of hard and soft photons are not shown in Fig. 1.

We would like to examine next under which conditions the non-linear loop operates. There are two conditions on the energies, that must be simultaneously satisfied. The first is the *feedback criterion* for photon quenching. This can be derived from the requirement that the magnetic field is strong enough so that the synchrotron photons of the produced pairs are above the threshold for photon-photon absorption on the hard photons. This leads to the condition for the magnetic field in the source $b > 8\epsilon_h^{-3}$ (SK07; PM11). The last relation combined with eqs. (2), (3) and (9) sets a lower limit to the magnetic field strength which depends only on γ_p

$$b \gtrsim b_q = \left[\frac{\sqrt{8}}{\eta_p^3} \left(\frac{m_e}{m_p} \right)^3 \right]^{1/2} \gamma_p^{-3/2}. \quad (10)$$

The second is that the energy of the soft photons is high enough for the production of pions in interactions with the protons, i.e., the relation

$$\frac{\epsilon_s \gamma_p \geq m_\pi}{m_e} \quad (11)$$

should hold. This sets another lower limit to the magnetic field strength given by

$$b \gtrsim b_\pi = \left(4 \frac{m_\pi}{m_e} \right)^{1/3} \left(\eta_p \frac{m_p}{m_e} \right)^{-4/3} \gamma_p^{-5/3}. \quad (12)$$

It is interesting to note that both b_q and b_π depend only on γ_p . Clearly, in order for non-linearity to appear in the system, the (normalized) magnetic field of the source

should satisfy the condition

$$b \geq \max(b_q, b_\pi). \quad (13)$$

This is not a strict limit. For instance, if $\gamma_p = 10^8$ one finds that $B_q = 0.04$ G and $B_\pi = 0.03$ G. Thus, magnetic fields of the order of 1 Gauss can easily satisfy condition (13). Perhaps more limiting are other various effects, that we proceed to discuss next:

(i) Photon quenching is based on the premise that soft photons start building in the system once the hard photons are above a certain critical luminosity, ℓ_h^{cr} . The idea is that hard photons are absorbed on the automatically created soft photons; the produced pairs emit more soft photons through synchrotron radiation which causes more pair production on the hard photons etc. However, in the present situation, the existence of an external photon population complicates the picture as the hard photons might pair produce on them, in parallel to the internally built soft photon population. This can act as a stabilizing factor, as it can inhibit the soft photon build-up in the system. This complication can be avoided if one assumes that the relation $\epsilon_h \epsilon_o < 2$ holds, i.e., that collisions between the two photon populations are below the threshold for pair-production. Since only ϵ_h depends on B and γ_p , one can find values for one of these parameters, in order $\epsilon_h \epsilon_o < 2$ to hold (see also §3). In the analytical treatment of the next section we will first start with this assumption but later we will relax this and study the effects, that the hard photon pair production on the external ones has on the dynamics of the system.

(ii) As the soft photons start building up, the secondary electron-positron pairs that produce them will start losing energy gradually through inverse Compton scattering instead of synchrotron radiation. This means that the photon quenching loop could become less efficient, because not all of the secondary electron luminosity will end up in the energy bin ϵ_s . This effect might become important near saturation, i.e., when the soft photon luminosity reaches its maximum value. As a first step, we will ignore inverse Compton scattering in our analytical treatment. Then, we will include it in an approximate manner to determine its effects. Finally, we will take this fully into account in our numerical treatment in §5.

(iii) The exact nature of the external photon density in the source was of no importance so far. As a first order approximation to the problem, we neglect proton synchrotron radiation, assuming that the initial photon distribution is purely external. Under this assumption, both the external photon number density n_{ex} and energy ϵ_o are treated as free parameters, instead of being determined by source properties, as the magnetic field B and the proton energy $\gamma_p m_p c^2$. However, in §5, where numerical solutions of the full problem are presented we replace the external source of photons by the proton synchrotron radiation.

(iv) In the analysis above the role of the hard photons was given to the synchrotron photons of the charged pion decay. Without loss of generality we could also assign them to π^0 initiated secondaries: Assuming that there is equipartition between the produced γ -rays from a π^0 -decay and that the

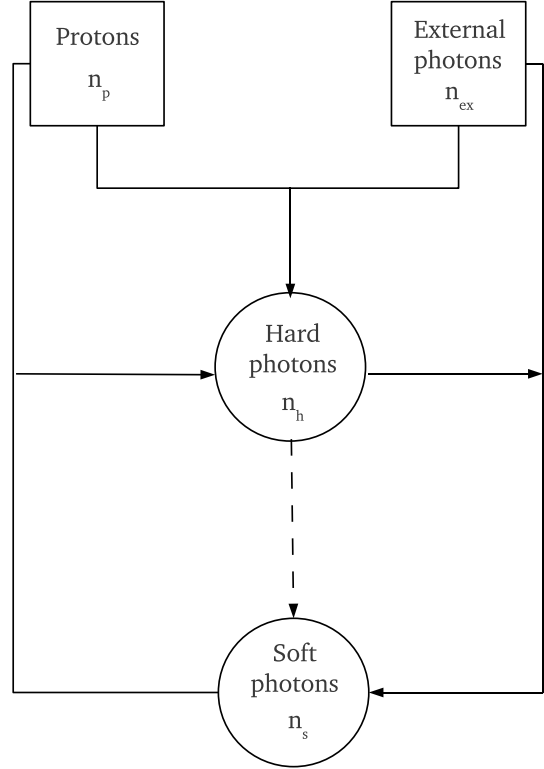


Figure 1. Schematic diagram of the operating loop of processes between protons and photons.

inelasticity parameter is about the same as that for charged pion decay, we can write in full analogy to eq. (2)

$$\epsilon_\gamma \approx 2\eta_p \gamma_p \frac{m_p}{m_e}. \quad (14)$$

These are extremely hard γ -rays and will always be above the threshold for pair production on the external photons ϵ_o . The produced pairs will have energy $\gamma_{e,\pi^0} = \epsilon_\gamma/2$ that is exactly the energy of the injected pairs through charged pion decay (c.f. eq. (2)). Therefore, both charged and neutral pions decay and produce pairs of the same energy, that could by synchrotron providing the hard photon emission.

3 ANALYTICAL APPROACH

3.1 Simplified equations

In the most general case, the hadronic system consists of three species of particles, namely protons, electrons and photons. In order to be described, the kinetic equations for the particles must be solved (Mastichiadis & Kirk 1995). Their generic form is:

$$\frac{\partial \tilde{n}_i}{\partial t} + \frac{\tilde{n}_i}{t_{i,esc}} = \tilde{L}^i + \tilde{Q}^i, \quad (15)$$

where the index i can be one of the subscripts ‘p’, ‘e’ or ‘ γ ’ referring to protons, electrons and photons respectively. The operators \tilde{L}^i and \tilde{Q}^i denote the losses and injection terms respectively, whereas $\tilde{n}_i/t_{i,esc}$ is just the escape term from

the source, with each species having its own escape time $t_{i,\text{esc}}$. For photons the relation $t_{\gamma,\text{esc}} = t_{\text{cr}} = R/c$ holds, whereas for protons we adopt $t_{p,\text{esc}} = 10^3 t_{\text{cr}}$ throughout the present work. The explicit expressions of the operators can be found in Mastichiadis & Kirk (1995) and Mastichiadis et al. (2005) – henceforth MK95 and MPK05 respectively.

The unknown functions to be determined are the number densities \tilde{n}_i , that can be normalized as follows:

$$\tilde{n}_p(\tilde{E}_p, \tau) = \frac{n_p(\gamma_p, \tau)}{\sigma_T R m_p c^2} \quad \text{with } \gamma_p = \frac{\tilde{E}_p}{m_p c^2} \quad (16)$$

$$\tilde{n}_e(\tilde{E}_e, \tau) = \frac{n_e(\gamma, \tau)}{\sigma_T R m_e c^2} \quad \text{with } \gamma = \frac{\tilde{E}_e}{m_e c^2} \quad (17)$$

$$\tilde{n}_\gamma(\tilde{\epsilon}_\gamma, \tau) = \frac{n_\gamma(\epsilon_\gamma, \tau)}{\sigma_T R m_e c^2} \quad \text{with } \epsilon_\gamma = \frac{\tilde{\epsilon}_\gamma}{m_e c^2}. \quad (18)$$

Time τ is normalized to the crossing time of the source t_{cr} , i.e., $\tau = t/t_{\text{cr}}$. From this point on, we adopt working with dimensionless quantities.

For the purposes of an analytical treatment, we make two major simplifications:

(i) Since electron cooling can be considered fast for typical values of the system's parameters (see also §2), we can neglect the equation of the electrons.

(ii) We simplify the equations describing the physical system to such a point as to retain only the key processes.

Thus, we assume a constant monoenergetic injection of protons $Q_{p0}(\gamma_p)$ into a spherical source of radius R and embedded magnetic field B . We assume also a monoenergetic distribution of external photons n_{ex} at energy $\epsilon_o = \gamma_p^{-1} \frac{m_\pi}{m_e}$, that acts as a target for high energy protons. We note that initially, n_{ex} is the only distribution of low energy photons present in the source. Charged pions produced by proton-photon pion processes, decay into electron-positron pairs with Lorentz factor $\gamma_{e,\pi}$ (see eq. (2)), that emit through synchrotron radiation, hard photons with corresponding number density $n_h(\epsilon_h)$. In order to ensure that inverse Compton scattering of the external photons by the aforementioned electrons is not as important as synchrotron cooling, and therefore can be safely neglected, we assume that $u_{\text{ex}} \ll u_B$ or equivalently $\ell_{\text{ex}} \ll \ell_B$, where u_i and ℓ_i are the energy densities and compactnesses respectively. At this point, it is useful to define the different compactnesses that appear in the present work:

$$\ell_i = \frac{\epsilon_i n_i}{3}, \quad i = s, h, \text{ex} \quad (19)$$

$$\ell_p = \frac{\gamma_p n_p}{3} \quad (20)$$

$$\ell_B = \sigma_T R \frac{u_B}{m_e c^2}. \quad (21)$$

In our treatment, secondary electrons do not affect the dynamics of the system. They rather play an intermediate role for transferring energy from hard photons to lower energy photons. We examine separately the hard and soft photon populations, n_h and n_s respectively, by writing a kinetic equation for each one of them. Thus, the quantities to be determined now, are n_p , n_h and n_s . The physical processes to be included into the simplified version of equations are:

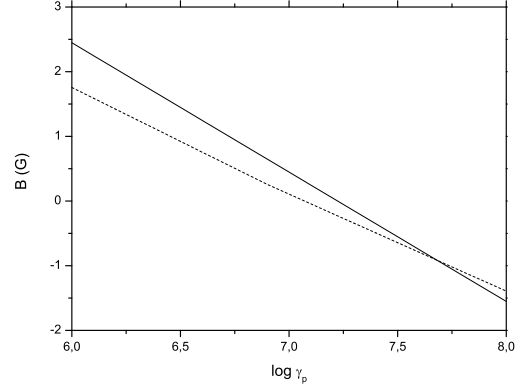


Figure 2. Upper (solid line) and lower (dashed line) limit of the magnetic field, where the lower limit is given by $\max(B_q, B_\pi)$ (see eq.(13)). Any value of the magnetic field that lies below the solid and above the dashed line, does not allow absorption of hard photons by the external ones. The lines are drawn for the minimum energy of external photons that satisfies the energy threshold for the photopion process, i.e. $\epsilon_o = \frac{m_\pi}{m_e \gamma_p}$.

(i) Constant proton injection Q_{p0} and proton escape $L_{\text{esc}}^p = -n_p/\tau_p$, that act as a source and a loss term respectively in the proton equation.

(ii) Proton-photon pion production, that acts as a loss term for protons $L_{p\gamma \rightarrow p\pi}^p$ and as an injection term for hard photons $Q_{p\gamma \rightarrow p\pi}^h$.

(iii) Photon-photon pair production, that acts as an absorption term for hard photons $L_{\gamma\gamma}^h$ and as an injection term for soft photons $Q_{\gamma\gamma}^s$.

(iv) Photon escape from the source in a crossing time, i.e., $L_{\text{esc}}^\gamma = -n_p$.

Under these considerations, the simplified kinetic equations for each species are given by:

$$\dot{n}_p = Q_{p0} - \frac{n_p}{\tau_p} + L_{p\gamma \rightarrow p\pi}^p \quad (22)$$

$$\dot{n}_h = -n_h + Q_{p\gamma \rightarrow p\pi}^h + L_{\gamma\gamma}^h \quad (23)$$

$$\dot{n}_s = -n_s + Q_{\gamma\gamma}^s. \quad (24)$$

The analytical study of the dynamics of the above set of equations can be simplified even further, if we assume that hard photons cannot be absorbed by the external ones (see point (i) of §2). To ensure this, we use for a given γ_p , such values of B that do not allow further absorption of hard photons. Thus, the condition $\epsilon_h \epsilon_o < 2$ should hold. This, combined with eq. (2) and (3) sets an upper limit for the magnetic field strength

$$b \lesssim b_\alpha = 2 \frac{m_e}{m_\pi} \left(\frac{m_e}{\eta_p m_p} \right)^2. \quad (25)$$

Equations (10), (12) and (25) can be combined in order to create a parameter space of allowed values of B for different proton energies – see Fig. 2. Solid line shows the upper limit of eq.(25), whereas dashed line shows the maximum value of the two lower limits given by eq. (13).

According to §2, if the compactness of hard photons is

below the critical value ℓ_h^{cr} , the instability that leads to an ‘automatic’ quenching of hard photons cannot grow. Thus, there is no injection of soft photons in the system and hard photons do not suffer any absorption. This situation corresponds to the linear regime described in §2.1. In this case, assuming that proton losses are catastrophic we can write $L_{p\gamma \rightarrow p\pi}^p = -\sigma_{p\gamma}^0 n_p n_{ex}$ and $Q_{p\gamma \rightarrow p\pi}^h = An_p n_{ex}$. The set of equations (22)-(24) degenerates into a system of two equations (S1):

$$\dot{n}_p = Q_{po} - \frac{n_p}{\tau_p} - \sigma_{p\gamma}^0 n_p n_{ex} \quad (26)$$

$$\dot{n}_h = -n_h + An_p n_{ex}. \quad (27)$$

The normalization constant A of the injection term in the hard photon equation above, is found after assuming that a fraction ξ_π of the total proton energy goes to secondary electrons, that radiate further all their energy through synchrotron producing the hard photons. Under these considerations, one finds that $A = \xi_\pi \frac{\sigma_{p\gamma}^0 m_p \gamma_p}{m_e \epsilon_h}$. The steady state solution of system S1 is

$$n_p^{ss} = \frac{Q_{po}}{G_p} \quad (28)$$

$$n_h^{ss} = An_p n_{ex}, \quad (29)$$

where $G_p = \frac{1}{\tau_p} + \sigma_{p\gamma}^0 n_{ex}$. Two limiting cases can be implied by the form of G_p :

- Proton escape is more significant than proton cooling on the external photons, i.e., $\sigma_{p\gamma}^0 n_{ex} \ll 1/\tau_p$. In this limit, the steady state solution for hard photons is proportional to the product $Q_{po} n_{ex}$. One can find a combination of values for Q_{po} and n_{ex} that lead to $\ell_h > \ell_h^{cr}$. For example if proton cooling is not efficient in injecting hard photons into the system because of a low n_{ex} , a high value of the proton injection rate is needed and vice versa.

- Proton cooling on the external photons is more significant than proton escape, i.e., $\sigma_{p\gamma}^0 n_{ex} \gtrsim 1/\tau_p$. In this limit, $n_h^{ss} \propto Q_{po}$. Thus, the system can become supercritical for a high enough value of the proton injection rate.

So far, the proton-photon system operates in a linear ‘subcritical’ regime with a very well described behaviour. In order to investigate how the non-linear terms affect the evolution of the system, we will focus only on cases where quenching is relevant. If hard photons are being injected into the system with $\ell_h^{inj} > \ell_h^{cr}$, then a soft photon population $n_s(\epsilon_s)$ appears because of the quenching of the γ -rays and the system becomes ‘supercritical’. In this case an additional equation for the soft photons is required. Thus, the set of equations (26)-(27) becomes (system S2):

$$\dot{n}_p = Q_{po} - \frac{n_p}{\tau_p} - \sigma_{p\gamma}^0 n_p n_{ex} - \sigma_{p\gamma}^0 n_p n_s \quad (30)$$

$$\dot{n}_h = -n_h + An_p n_{ex} + An_p n_s - C_h n_s n_h \quad (31)$$

$$\dot{n}_s = -n_s + C_s n_s n_h, \quad (32)$$

where

$$C_h = \frac{\sigma_{\gamma\gamma}^{(s)}}{\epsilon_h \epsilon_s} \quad \text{and} \quad C_s = \frac{\sigma_{\gamma\gamma}^{(s)}}{\epsilon_s^2}. \quad (33)$$

The term $\sigma_{\gamma\gamma}^{(s)}$ that appears in expressions (33) is given by

$$\sigma_{\gamma\gamma}^{(s)} = \epsilon_h \epsilon_s \sigma_{\gamma\gamma}(\epsilon_h \epsilon_s) \quad (34)$$

with the exponent ‘s’ denoting the absorption on the soft photons and $\sigma_{\gamma\gamma}$ the cross section of photon-photon absorption, measured in units of the Thomson cross section σ_T . Here and throughout this work, we use the approximate expression of Coppi & Blandford (1990):

$$\sigma_{\gamma\gamma}(x) = 0.652 \frac{(x^2 - 1)}{x^3} \ln(x) H(x - 1), \quad (35)$$

where x is the product of the dimensionless photon energies and $H(x)$ is the Heaviside step function. Since in our analysis we have assumed monoenergetic photon distributions and a cross section approximated by a step function, $\sigma_{\gamma\gamma}^{(s)}$ in definitions (33) is just a constant, that takes different values for different pairs of photons. The last terms in the right hand side of eqs. (31) and (32) account for the photon-photon absorption. The created pairs are the intermediate products that transport their energy through synchrotron radiation to soft photons. The constants C_h and C_s given above are determined by energy conservation. As far as the soft photons produced have enough energy to satisfy the energy threshold for photopion interactions, (see relation (11)), they can act as an additional target for protons. This explains the last term in the right hand side of eq. (30). This additional sink term of protons has a corresponding injection term $An_p n_s$, that appears in eq. (31).

We note that an expression of the critical compactness for the automatic quenching of hard photons has been presented by SK07 and PM11. In the present analysis we have made certain simplifying assumptions that differ from those in the aforementioned papers. Thus, for reasons of consistency, we calculate the modified expression of ℓ_h^{cr}

$$\ell_h^{cr} = \frac{\epsilon_h}{3C_s} \quad (36)$$

(see Appendix C for the derivation).

3.2 Dynamical study of the system

After having set the framework of the physical problem and clarified our assumptions, we proceed to investigate the mathematical properties of the system.

Setting in equations (30)-(32) the time derivatives equal to zero we can determine the possible steady states, that actually are the ‘fixed points’ of the dynamical system. The system of equations S2 has one or three fixed points depending on the existence or not of the coupling terms between hard and soft photons. We will treat the system of equations that obtains three fixed points, since this can in principle show non-linear temporal behaviour.

The first fixed point P_1 is just the steady state solution presented in the previous section, i.e., $P_1(n_h^{ss}, 0, n_p^{ss})$. Perturbations of this steady state solution can either grow or decay with time as $e^{s\tau}$. In the first case, the fixed point P_1 is unstable whereas in the second case it is stable (see Appendix A for a detailed analysis). The growth or decay rate s of the perturbations as a function of the proton injection rate, for a fixed external number density, is shown in Fig. 3. It is interesting to note that the exponent s for the growing solutions depends strongly on Q_{po} , whereas the respective

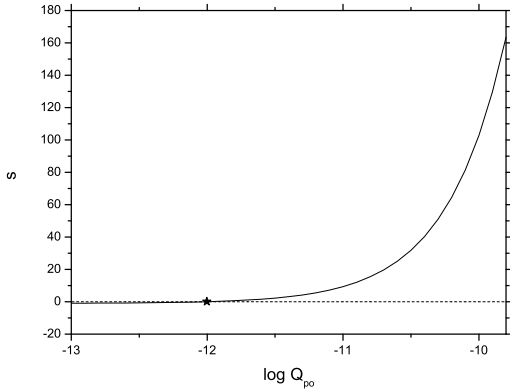


Figure 3. Growth/decay rate of the perturbed proton and photon densities from the steady state P_1 as a function of the proton injection rate. Above a certain value of Q_{po} , that is denoted with a star, only growing perturbations exist. Parameters used for this plot are: $B = 0.7$ G, $\gamma_p = 2 \times 10^7$, $\epsilon_o = \gamma_p^{-1} \frac{m_\pi}{m_e}$ and $n_{ex} = 2$.

one for the decaying solutions is rather insensitive to Q_{po} and close to -1 , denoting the free escape of the produced soft photons in a crossing time. The star denotes the critical value of the proton injection rate, Q_{po}^{cr} , above which $s > 0$ and an automatic build-up of soft photons in the system is possible. This value depends on the external photon density as:

$$Q_{po}^{cr}(n_{ex}) = \frac{1}{C_s A n_{ex}} \left(\frac{1}{\tau_p} + \sigma_{p\gamma}^0 n_{ex} \right). \quad (37)$$

Low values of n_{ex} suggest inefficient proton cooling and therefore inefficient injection of hard photons – see eqs. (26)–(27). Only if the injection rate of protons in the source is high, can the hard photon compactness increase sufficiently leading the system to instability. In other words, for a given n_{ex} one can find always a sufficiently high Q_{po} in order to make the system unstable. Q_{po}^{cr} is directly related to a critical proton number density n_p^{cr} given by

$$n_p^{cr} = \frac{Q_{po}^{cr}}{1/\tau_p + \sigma_{p\gamma}^0 n_{ex}}. \quad (38)$$

Thus, the problem of choosing a suitable pair of values (Q_{po}, n_{ex}) that lead the system to instability, can be transferred to the problem of loading the source with a critical proton content. Let us now consider the inverse of the above statement: *if the injection rate of protons is given, is there any value of n_{ex} that will make the system unstable?* In this case, we find that the external number density must satisfy the following condition:

$$n_{ex} \gtrsim \frac{1/\tau_p}{C_s A Q_{po} - \sigma_{p\gamma}^0}, \quad (39)$$

with the constraint $Q_{po} > \frac{\sigma_{p\gamma}^0}{C_s A}$. Thus, for low enough proton injection rates, the system cannot become unstable. The above remarks lead to the conclusion that, between the two parameters, Q_{po} and n_{ex} , the fundamental one in making the system unstable is the proton content of the source.

When the initial growth of the perturbations is ensured,

the subsequent behaviour of the system depends on the properties of the second fixed point P_2 . The system can either reach the steady state P_2 or vary periodically, making a limit cycle in phase space. This behaviour can be predicted by calculating the eigenvalues of the matrix M_2 of the linearized system of equations, near the point P_2 . For different values of the physical parameters of the problem, we find always one real negative eigenvalue, λ_1 . The two remaining eigenvalues $\lambda_{2,3}$ can either be complex conjugates or both real and negative (see Appendix B for more details). Table 1 summarizes the dynamical behaviour of the system. We note that, for the terminology regarding the classification of a fixed point of a three-dimensional system, we have adopted the one presented in Theisel, Weinkauff, Hege, & Seidel (2003).

Eigenvalues	Classification of point P_2	Dynamical behaviour
$\lambda_i < 0$, for $i = 1, 3$	attracting <i>node</i>	steady state
$\lambda_1 < 0$, $\lambda_2 = \lambda_3^*$	<i>focus</i>	
$\text{Re}(\lambda_2) = \text{Re}(\lambda_3) > 0$	repelling saddle	limit cycles
$\text{Re}(\lambda_2) = \text{Re}(\lambda_3) < 0$	attracting	damped oscillations

Table 1: Classification of the fixed point P_2 and of the expected dynamical behaviour of the system, based on an eigenvalue/eigenvector analysis of the corresponding matrix M_2 .

It is interesting to investigate how the two main parameters of the physical problem, i.e., the proton injection rate Q_{po} and the external number density n_{ex} , are related to the dynamical behaviour of the system. For this purpose, we calculate the eigenvalues of matrix M_2 around the fixed point P_2 for different values of Q_{po} and n_{ex} , having first ensured that the fixed point of the steady state P_1 is unstable (see Appendix A). The results are presented in the next two paragraphs.

3.2.1 Dependence on proton injection rate

We assume first that the external density n_{ex} is fixed to a certain value and study the effects of the injection rate Q_{po} . Figure 4 shows the calculated eigenvalues $\lambda_{2,3}$ for different values of Q_{po} . The conclusions drawn from it can be summarized in the following points:

(i) Starting with low values of Q_{po} , we find that $\lambda_3 = \lambda_2^*$. As long as $\text{Re}(\lambda) > 0$, point P_2 acts as a repelling focus - saddle point. Having also ensured that the fixed point of the steady state P_1 is unstable, the system follows in phase space a closed periodic trajectory, i.e., a limit cycle that is moreover stable.

(ii) For higher values of the proton injection rate we find complex eigenvalues with $\text{Re}(\lambda) < 0$. Therefore, the point P_2 acts as an attracting focus - saddle point. In this case, the system settles down in a new steady state (given by the fixed point P_2). In phase space, this cor-

responds to a ‘spiraling’ trajectory ending at the fixed point.

(iii) Finally, for even higher values of Q_{po} both eigenvalues become real and negative. Point P_2 can be characterized as an attracting node. The physical system reaches the new steady state very fast, showing no oscillations.

An example of such a transition in the dynamics of the system, is shown in figures 5 and 6. The solution shown with dashed-dotted line corresponds to a limit cycle case with period $\sim 170 t_{\text{cr}}$. For reasons of clarity, Fig. 5 zooms in the early time behaviour of the system. Therefore, only the first and a half cycle of the periodic solution is shown. The solutions presented in the aforementioned figures are found after integrating the system of equations S2 with initial conditions $n_{\text{h}}(0) = n_{\text{p}}(0) = 0$ and $n_{\text{s}}(0) = \epsilon$, with $\epsilon \rightarrow 0$ indicating an initial perturbation of soft photons in the source. The parameters used ensure that at some point the compactness of hard photons becomes larger than $\ell_{\text{h}}^{\text{cr}}$. Each of the values of Q_{po} used in this example corresponds to a different point of Fig. 4. The conclusion is that the temporal behaviour of the system is very sensitive with respect to the proton injection rate.

For reasons of mathematical consistency we make also the following remark: As the proton injection rate increases, the real part of the complex eigenvalues changes sign and from positive it turns into negative. At this transition a second unstable limit cycle⁴ surrounding the fixed point P_2 appears inside the stable limit cycle (see point (1) above). An integration of the equations of S2 with initial conditions lying outside the stable limit cycle would show that the system falls onto this cycle instead of ‘spiraling’ down to the fixed point, as one would expect according to point (2). As the varying parameter Q_{po} increases further, $|\text{Re}(\lambda_{2,3})|$ increases too and the unstable limit cycle approaches the stable one. At some value, which for the specific example of Fig. 4 is $\log Q_{\text{po}} = -10.9$, the two limit cycles coalesce and the system undergoes a bifurcation⁵ since the phase space changes qualitatively. From this moment on the system can fall into the fixed point P_2 , as described in (2) above. Thus, the condition $\text{Re}(\lambda_{2,3}) < 0$ that occurs for $\log Q_{\text{po}} = -11.5$ in our example, does not ensure strictly speaking the damped oscillatory behaviour of the system.

It is beyond the scope of the present work to proceed into a detailed study of the bifurcation mentioned earlier, since for the initial conditions of physical relevance to our analysis, the existence of the bifurcation does not affect the qualitative features of the transition from the limit cycle phase to the damped oscillatory one.

3.2.2 Dependence on number density of external photons

In this section we show an example of the effects of the external number density n_{ex} on the dynamical properties of the system. An increase of the external number density leads

⁴ We note that the existence of the unstable limit cycle was found numerically while integrating the equations of system S2 and not analytically.

⁵ The existence of the bifurcation is not a characteristic property of the system for all values of the parameters. For example, if $n_{\text{ex}} = 10$ no bifurcation of this type is found.

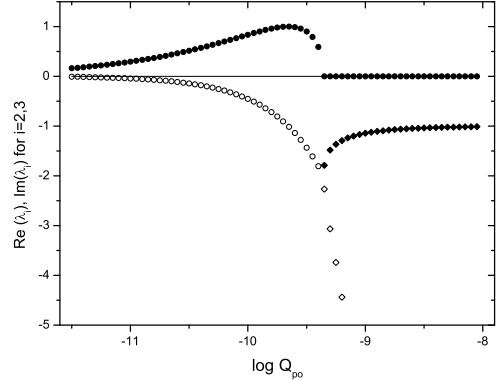


Figure 4. Plot of the two eigenvalues $\lambda_{2,3}$ for $n_{\text{ex}} = 2$ as a function of the injected proton rate. As long as the eigenvalues are complex conjugates, their real and imaginary parts are shown with open and filled circles respectively. At a certain value of Q_{po} both eigenvalues become real and negative (open and filled diamonds). The solid line corresponds to the null value. The other parameters used are the same as in Fig. 3.

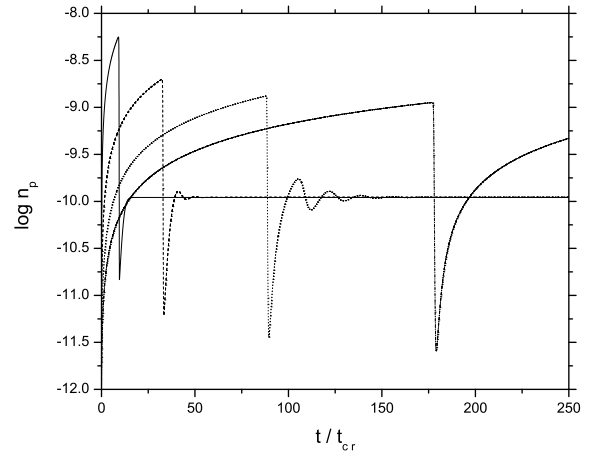


Figure 5. Time evolution of the proton distribution for different values of the proton injection rate $\log Q_{\text{po}} = -11.5$ (dashed-dotted line), $\log Q_{\text{po}} = -10.8$ (dotted line), $\log Q_{\text{po}} = -10.2$ (dashed line) and $\log Q_{\text{po}} = -9.2$ (solid line). The initial conditions for each numerical run are $n_{\text{h}}(0) = n_{\text{p}}(0) = 0$ and $n_{\text{s}}(0) = \epsilon \rightarrow 0$. The number density of the external photon distribution is $n_{\text{ex}} = 2$ in all cases. All the other parameters used are the same as in Fig. 3.

to the same transition of the dynamical behaviour of the system, as the one described in the previous section. Figure 7 shows the calculated eigenvalues for a large range of n_{ex} extending up to high values. The qualitative features of this plot are the same as those of Fig. 4. One should keep in mind though, that the conclusions drawn from Fig. 7, regarding the dynamics of the system are not valid for the whole range of values of n_{ex} shown. The reason is the following: As n_{ex} increases, the compactness of the external photons ℓ_{ex} increases too. At some value, which for the specific example is just $n_{\text{ex}} = 35$, it becomes larger than the compactness of

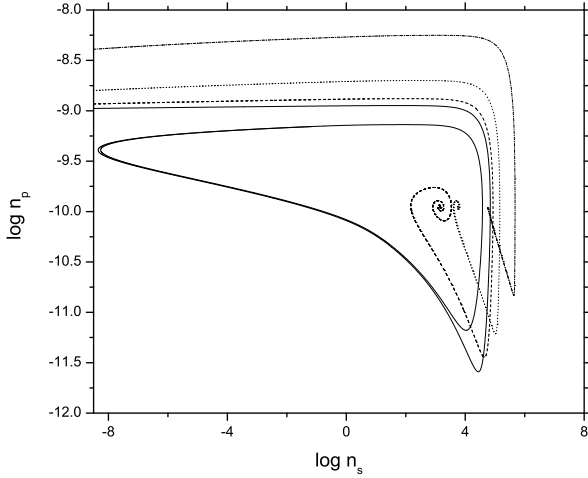


Figure 6. Two-dimensional plane of the phase space for different values of the proton injection rate $\log Q_{po} = -11.15$ (dashed-dotted line), $\log Q_{po} = -10.8$ (dashed line), $\log Q_{po} = -10.2$ (dotted line) and $\log Q_{po} = -9.2$ (solid line). Same parameters used as in Fig. 5.

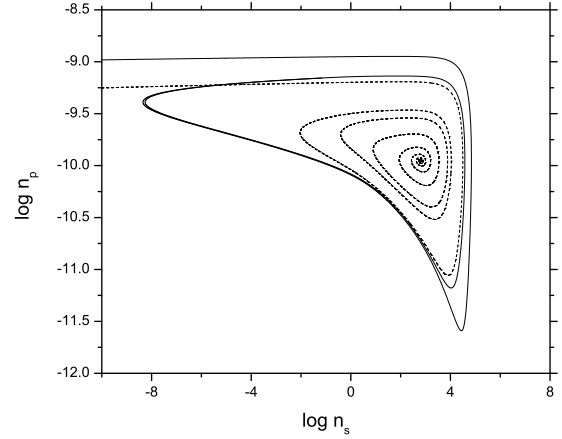


Figure 8. Two dimensional plane of the phase space for two values of the external number density $n_{ex} = 2$ (solid line) and $n_{ex} = 4$ (dashed line). The proton injection rate is $\log Q_{po} = -11.15$ in both cases. The initial conditions for each numerical run are $n_h(0) = n_p(0) = 0$ and $n_s(0) = \epsilon \rightarrow 0$. All other parameters used are the same as in Fig. 3.

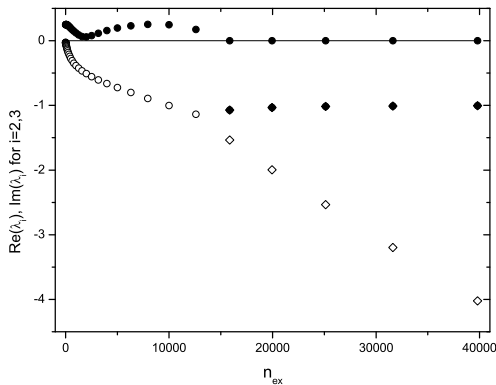


Figure 7. Plot of the two eigenvalues $\lambda_{2,3}$ as a function of the external number density n_{ex} for injected proton rate $\log Q_{po} = -11.15$. While the eigenvalues are complex conjugates, their real and imaginary parts are shown with open and filled circles respectively. At a certain value of n_{ex} both eigenvalues become real and negative (open and filled diamonds). The solid line corresponds to the null value. All other parameters used are the same as in Fig. 3.

the magnetic field $\ell_B = 1.6 \times 10^{-4}$. This means that the secondary electrons produced by the pion decay, cool preferably through inverse Compton scattering on the external photon field, rather than through synchrotron radiation. Thus, the system of equations S2 we used to make our mathematical analysis is physically not valid. However, aim of Fig. 7 is to simply show the mathematical similarities of this case with the previous one.

Figure 8 shows a two-dimensional plane of the phase space for two different values of the external density. All the other parameters are kept constant. The corresponding time evolution of the proton distribution is shown in Fig. 9.

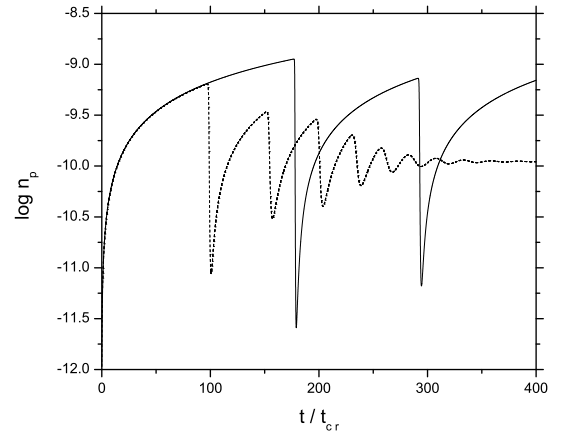


Figure 9. Time evolution of the proton number density for proton injection rate $\log Q_{po} = -11.15$ and two values of the external number density, i.e. $n_{ex} = 2$ (solid line) and $n_{ex} = 4$ (dashed line). The initial conditions for each numerical run are $n_h(0) = n_p(0) = 0$ and $n_s(0) = \epsilon \rightarrow 0$. All other parameters used are the same as in Fig. 3.

External photons act as a stabilizing factor for the system, since high enough values lead the system to a steady state.

4 ENHANCING NON-LINEARITY WITH ADDITIONAL PROCESSES

4.1 Photon-photon absorption by the external source

In the previous section, in order to avoid the appearance of more terms in the equations and be able to treat them analytically, we restricted our analysis to values of B taken

from the parameter space shown in Fig. 2 and to external photons having energy equal to the threshold energy for proton-photon pion processes. If one wishes to use values of the magnetic field more related to astrophysical sources or consider more energetic external photons, the absorption of hard photons on the external ones must be taken into account.

Thus, two more terms appear in the equations of hard and soft photons and the corresponding system now is (system S3):

$$\dot{n}_p = Q_{p0} - \frac{n_p}{\tau_p} - \sigma_{p\gamma}^0 n_p n_{ex} - \sigma_{p\gamma}^0 n_p n_s \quad (40)$$

$$\dot{n}_h = -n_h + A n_p n_{ex} + A n_p n_s - C_h n_s n_h - C'_h n_{ex} n_h \quad (41)$$

$$\dot{n}_s = -n_s + C_s n_s n_h + C'_s n_{ex} n_h, \quad (42)$$

where $C'_h = \frac{\sigma_{\gamma\gamma}^{(ex)}}{\epsilon_0 \epsilon_h}$ and $C'_s = \frac{\sigma_{\gamma\gamma}^{(ex)}}{\epsilon_0 \epsilon_s}$. These terms are derived using energy conservation considerations as in §3. The index ‘ex’ is used to remind that the photon-photon cross section has a different value depending on whether the absorbing targets are the soft or the external photons.

The additional coupling terms make now an analytical study as the one presented in §3 cumbersome. Thus, all the results presented in this section are derived after solving numerically the stiff set of equations S3.

Our solutions indicate that these extra terms do not change, at least qualitatively, the validity of the results of the previous section. Increasing either Q_{p0} or n_{ex} above a certain value, forces the system to fall into a steady state rather than oscillate. As a first step, we compare two cases: (i) with and (ii) without the extra terms of absorption. In both cases we have used $B = 0.7$ G, $\gamma_p = 2 \times 10^7$, $\log Q_{p0} = -11.15$ and $n_{ex} = 2$. What differs in the two cases are the external photon energies, that are taken to be (i) $\epsilon_0 = 100 \gamma_p^{-1} \frac{m_\pi}{m_e}$ and (ii) $\epsilon_0 = \gamma_p^{-1} \frac{m_\pi}{m_e}$ respectively. Although the system shows is oscillatory in both cases, there is an important difference that is better displayed when the time evolution of the soft photon distribution is plotted (see Fig. 10). At early times, the soft photon number density evolves in the same way in both cases. However, in the first case the number of soft photons in the source does not reach a deep minimum as in the second case. This can be attributed to the existence of the additional linear injection term of soft photons, i.e., $+C'_s n_{ex} n_h$. Since the latter depends only on one time-varying parameter (n_h), it adds soft photons into the system at a non negligible rate, in contrast to the non-linear term $+C_s n_s n_h$, that depends quadratically on the time-varying densities.

This is also reflected on the shape of the limit cycles in the plane $n_p - n_s$ of the phase space, which now appear tighter than before. This is shown in Fig. 11.

As already discussed in section 2.2, the existence of an initial external photon distribution makes the role of quenching less clear. However, the way the equations of system S3 are written, allows us to study separately the linear and non-linear absorption of hard photons by artificially deleting the non-linear terms of quenching in the equations of hard and soft photons, i.e., $-C_h n_s n_h$ and $+C_s n_s n_h$ respectively. For this purpose we examine two cases, that differ only at the proton injection rate. Figure 12 shows the hard photon compactness as a function of time for both cases, with panel

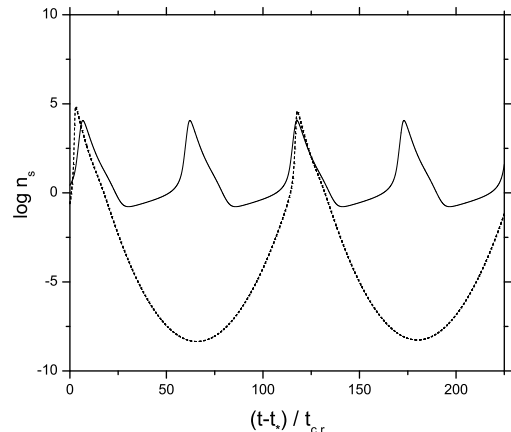


Figure 10. Time evolution of the soft photon distribution n_s in the case where hard photons are being absorbed on both the external and the soft photons (solid line) and in the case where they are being absorbed only on the latter (dashed line). Time is measured with respect to t_* , that corresponds to the end of a transient phase that the system goes through, before it settles to its periodic state. For reasons of clarity, the transient phase is not shown. For the parameters used, see text.

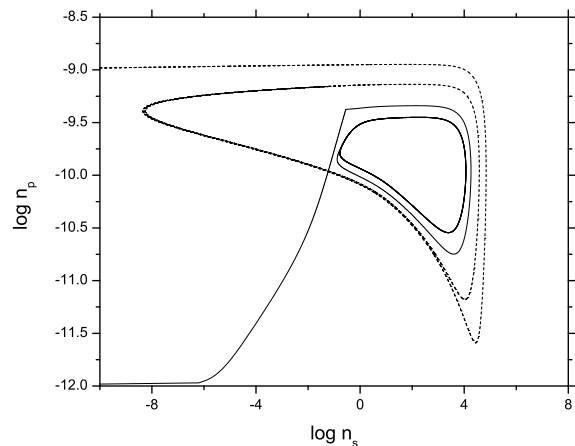


Figure 11. Two dimensional plane $\log n_p - \log n_s$ of the phase space in the case where hard photons are being absorbed on both the external and the soft photons (solid line) and in the case where they are being absorbed only on the latter (dashed line). Same parameters used as in Fig. 10.

(a) corresponding to the case with the larger proton injection rate. The horizontal dotted line corresponds to ℓ_h^{cr} , the solid line shows ℓ_h when both absorption channels operate, whereas the dashed line shows ℓ_h when we ignore the soft photons produced due to non-linear quenching. Comparison of the solid and dashed lines leads to the conclusion that the automatic quenching of hard photons becomes dominant in the dynamics of the system from the instant that $\ell_h \gtrsim \ell_h^{cr}$. Thus, even if quenching cannot be distinguished from the linear absorption when both operate, ℓ_h^{cr} still remains an intrinsic property of the system.

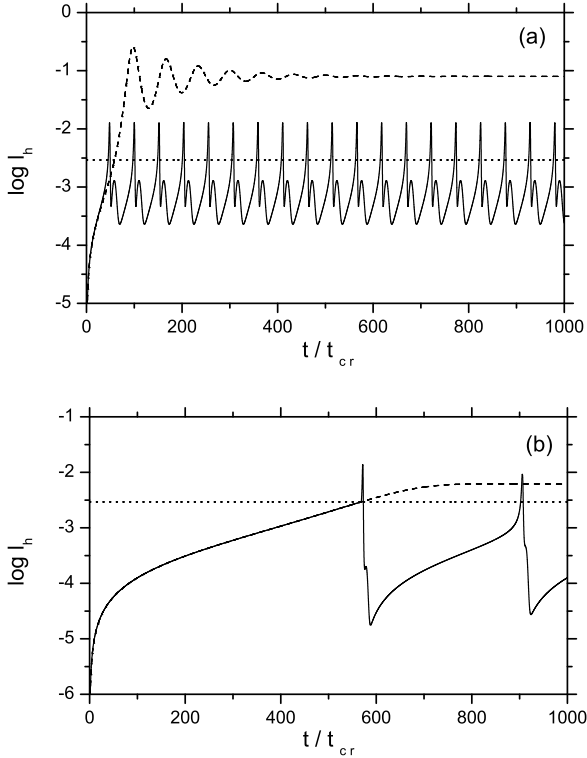


Figure 12. Time evolution of hard photon compactness when (i) γ -rays are being absorbed both on external and on automatically produced soft photons (solid lines) and when (ii) the non-linear terms of absorption are artificially omitted (dashed lines). The dotted line in both panels corresponds to ℓ_h^{cr} . The cases presented in panels (a) and (b) differ only at the proton injection rate, which is taken to be $Q_{po} = 3.2 \times 10^{-11}$ and $Q_{po} = 4 \times 10^{-12}$ respectively. The rest of the parameters used in both panels are the same and equal to: $B = 0.75$ G, $\gamma_p = 2.65 \times 10^7$, $\epsilon_o = 10^{-5}$ and $n_{ex} = 1$.

Another conclusion drawn from Fig. 12 is that even in the absence of automatic quenching the system can exhibit damped oscillations. These example cases show clearly that the large-period limit cycle behaviour exhibited when automatic quenching operates in parallel to the linear one, is replaced by an exponential growth that saturates, in the case where quenching is artificially omitted. On the other hand, the small-period limit cycle behaviour is replaced by damped oscillations of small amplitude. In other words, the combination of linear and non-linear absorption of γ -rays seems to intensify the temporal variability of the system. Finally, the absorption of hard photons is more efficient in the case where both the linear and non-linear channels of absorption operate than in the case where hard photons are being absorbed only on the external photon population. This can be deduced from the fact that, in the former case the averaged ℓ_h over a period is suppressed by at least one order of magnitude (see solid and dashed lines in panel (a) of Fig. 12).

Two operating regimes of the system, each of them having its own properties, can be defined, depending on the relative strength of the two absorbing channels: (i) a linear and (ii) a non-linear one. While being in the linear regime,

ℓ_h grows at first exponentially and eventually saturates. The transition from the linear to the non-linear operating regime depends on the external number density or equivalently on the optical depth τ_{ex} for absorption of hard photons on the external ones. In our analysis, τ_{ex} is simply given by

$$\tau_{ex} = \sigma_{\gamma\gamma}(\epsilon_h \epsilon_o) n_{ex}(\epsilon_o). \quad (43)$$

For small optical depths, i.e., $\tau_{ex} \ll 1$, this transition is abrupt in the sense that the system changes its temporal behaviour completely. From the instant that automatic quenching becomes the dominant channel for absorption, the system exhibits limit cycles of large period and amplitude. On the other hand, for large optical depths, i.e., $\tau_{ex} \gtrsim 1$, the transition is smooth, since the system shows no limit-cycle behaviour. The non-linearity in the temporal behaviour becomes evident by damped oscillations that reach a steady state in a few crossing times. Thus, the flaring behaviour of the system can be severely suppressed whenever the optical depth for absorbing γ -rays on external photons is large. Panels (a) and (b) of Fig. 13 show ℓ_h as a function of time for two cases, where $\tau_{ex} = 1.3$ and 0.13 respectively. In each panel, lines of different type denote different proton injection rates. The lightcurves depicted with dashed-dotted lines in both panels are obtained while the system operates in its linear regime. The dotted lightcurves exemplify the transition to non-linearity, which is more abrupt for the case in panel (a) than the corresponding in panel (b).

A new feature that appears through the study of system S3 is the dependence of the period T , if this exists, on the energy of the external photons ϵ_o . This is exemplified in Fig. 14, where the period of the oscillations varies with ϵ_o almost like $T \propto 1/\sigma_{\gamma\gamma}(\epsilon_o)$ – see eq. (35). The minimum period is found at ϵ_o that corresponds to the maximum value of the cross section for photon-photon absorption; for this value the absorption of hard photons becomes most effective. The dashed line shows the dependence of the period on ϵ_o for a higher density of external photons. In this case a gap appears for values of ϵ_o that correspond to high values of the cross section around its peak. The evolution of the system there, is characterized by damped oscillations that lead eventually to a steady state. This result is to be expected within our analysis of §3. We remind that the system passes through well-defined stages, as one of the parameters Q_{po} or n_{ex} increases: oscillations with large period \rightarrow oscillations with small period \rightarrow damped oscillations leading to a steady state.

The fact that we find a clear analogy between the period and the inverse of the cross section for photon-photon absorption is a direct consequence of the simplifications we have made in the problem so far. However we note that, if were to relax our assumptions, i.e., use full expressions for the cross sections and emissivities, and treat the problem numerically, we would still have retained the basic conclusions of Fig. 14.

We have also found that the period of the limit cycles depends not only on ϵ_o but also on other parameters, that affect the value of the cross section of photon-photon absorption even indirectly, as the magnetic field strength or/and the proton energy (see eqs. (2), (3) and (9)). The trend is the same as the one shown in Fig. 14, where ϵ_o in the horizontal axis should be replaced by the corresponding varying parameter.

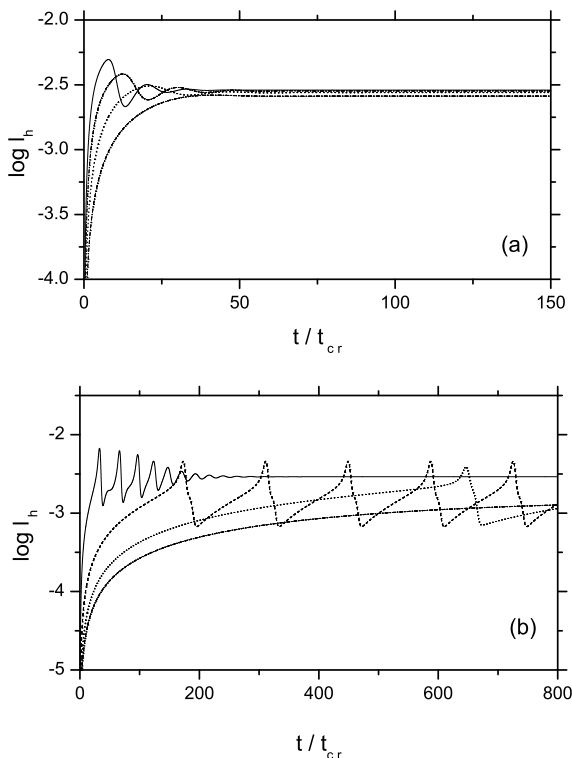


Figure 13. Hard photon compactness as a function of time for two cases with $\tau_{\text{ex}} = 1.3$ (panel a) and 0.13 (panel b). In both panels the different light curves are obtained by increasing the proton injection rate. The transition from the linear to the non-linear operating regime of the system is clearly seen. Specifically, for panel (a) we have used: $Q_{\text{po}} = 10^{-11}$ (dash-dotted line), 2×10^{-11} (dotted line), 4×10^{-11} (dashed line) and 8×10^{-11} (solid line). The corresponding values for panel (b) are: $Q_{\text{po}} = 10^{-12}$ (dash-dotted line), 1.6×10^{-12} (dotted line), 4×10^{-12} (dashed line) and 2.5×10^{-11} (solid lines). The rest of the parameters used are the same for both panels: $B = 0.75$ G, $\gamma_p = 2.65 \times 10^7$ and $\epsilon_o = 10^{-3}$.

4.2 Inverse Compton scattering

Thus far, we have assumed that the created pairs from photon-photon absorption act as an agent, transferring the energy from hard to soft photons through synchrotron radiation. However, if the compactness of soft photons becomes comparable or larger than the compactness of the magnetic field, i.e., $l_s \gtrsim l_B$, then there are two cooling channels for the secondary electrons: (i) the ‘synchrotron’ one that results to the production of soft photons ϵ_s and (ii) the ‘inverse Compton’ (ICS) one that results to the production of high energy photons ϵ_{ics} – note that in general $\epsilon_{\text{ics}} \neq \epsilon_h$. Thus, the energy lost by hard photons is only partially injected to the soft photon population. Because of this, the constant C_s of the injection term in eq. (42) should be replaced by

$$C_s^{\text{eff}} = C_s \frac{l_B}{l_B + 3l_s(1 + 4\epsilon_s\gamma_e)^{-3/2}}, \quad (44)$$

where $\gamma_e = \epsilon_h/2$ and the multiplication factor of l_s accounts approximately for the Klein-Nishina cutoff effect up to $\epsilon_s\gamma_e \lesssim 10^4$ (Moderski et al. 2005). Inspection of system S3

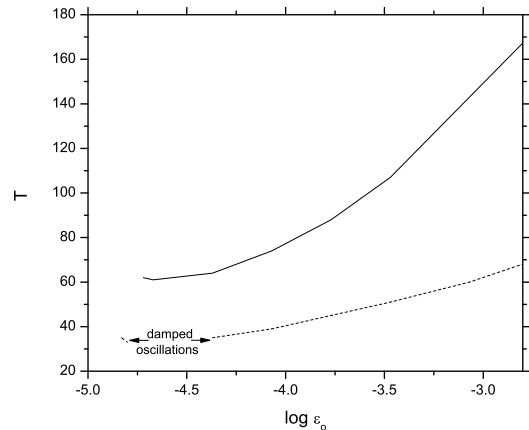


Figure 14. Dependence of the period T on the energy of the external photons ϵ_o for number densities $n_{\text{ex}} = 1$ (solid line) and $n_{\text{ex}} = 3$ (dotted line). The rest of the parameters used are: $Q_{\text{po}} = 10^{-10}$, $B = 3.57$ G, $\gamma_p = 9 \times 10^6$ and $\epsilon_o = 8 \times 10^{-5}$.

together with the expression (44) shows that the inclusion of ICS adds more non-linear terms to the problem.

It is beyond the scope of the present work to proceed to a semi-analytical study of the above system. However, it is worth mentioning some qualitative effects of ICS on the dynamics of the system. In general, ICS acts as a damping term for soft photons whenever $l_s \gtrsim l_B$.

Let us assume first, that we artificially switch-off ICS, and find a set of parameters that lead our system to a limit cycle behaviour as discussed in the previous section. If we keep the parameters fixed to these values and switch-on ICS, then there are three possible ways for the evolution of the system :

- (i) The limit cycle behaviour remains, although the system oscillates with a smaller period.
- (ii) The limit cycle behaviour is damped and the system finds its steady state after a number of oscillations.
- (iii) The system falls quickly into a steady state before showing any oscillations.

The resulting behaviour of the system depends on the ratio l_s/l_B and on whether or not the scatterings occur in the Klein-Nishina regime. Figure 15 exemplifies the above remarks. The solutions shown in Fig.15 are obtained after integrating the system of equations S3 and incorporating ICS in the approximate way described in this section. In both cases, the system starts with $l_s \ll l_B$ but eventually reaches a state where $l_s \gtrsim l_B$. The difference between the cases above is the parameter $x_{\text{ics}} = \epsilon_s\gamma_e$, that denotes how deep into the Klein-Nishina regime the scatterings occur. Cases presented in panels (a) and (b) correspond to values $x_{\text{ics}} = 7.6$ and 87 respectively. In the former case, the damping effect of ICS is evident, whereas in the latter case the system’s evolution is not much affected because of the suppression of the scatterings. A small decrease in the period and in the amplitude of the oscillations is however evident. In the following section, where we treat numerically the full problem, we present a case that exemplifies the effects of ICS.

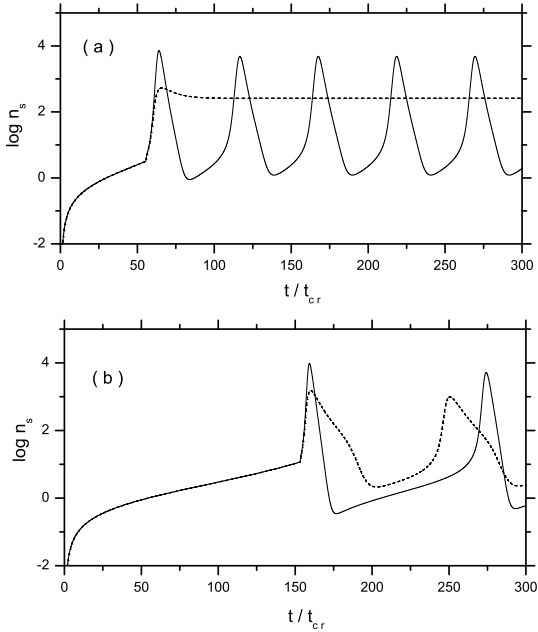


Figure 15. Soft photon density n_s as a function of time for proton Lorentz factors $\gamma_p = 2.1 \times 10^7$ and 2.65×10^7 (panels a and b respectively), derived for two cases: (i) ICS is artificially switched-off (solid lines) and (ii) ICS is taken approximately into account (dashed lines). Other parameters used for this plots are: $B = 0.75$ G, $\log Q_{po} = -11.15$, $n_{ex} = 2$ and $\epsilon_o = \gamma_p^{-1} \frac{m_\pi}{m_e}$.

5 NUMERICAL APPROACH

All of our previous results were verified in an independent way by using the numerical code described in MK95 after selectively omitting various processes, as to make the code analogous to the systems described in the previous section.

We proceed next to solve numerically the full system of eqs. (15). Our aim is to present only some characteristic examples which will support our previous analysis and show also the effects of the processes we have neglected in our analytical approach, most notably of inverse Compton scattering, on the dynamical behaviour of the system. We leave a comprehensive search of the parameter space for a future paper, where the interplay between proton injection and external photons will be fully addressed.

We have used the numerical code described in MK95 and MPK05 which has been updated as to make use of the full rates for the secondary electron-positron pairs and photon production in photopion interactions as obtained from the SOPHIA Monte Carlo code (Mücke et al. 2000). Details on these will appear elsewhere – Dimitrakoudis et al. in preparation; see also Dimitrakoudis et al. (to appear in 2012). Therefore the updated version of the code can treat accurately the two major hadronic processes, i.e., photopair and photopion, in addition to the leptonic ones. Given the difficulty that these two processes pose in modelling, we consider this as a major improvement.

We solve therefore three coupled equations, for protons, electrons and photons including all relevant processes between the three species – note that in the numerical code there is no need to treat the hard and soft photons through separate equations. Another difference with the analytical

treatment is that in place of the external photons we use the photons produced by the proton synchrotron radiation. This was done because this process can produce the seed photons self-consistently without the need of introducing more free parameters. Furthermore, the proton synchrotron radiation, for magnetic fields of ~ 10 G and protons with Lorentz factors $\gamma_p \gtrsim 10^6$ is produced mainly in the soft energy range of the spectrum and cannot/should not be neglected.

Fig. 16 shows four cases that differ only in the proton injection rate. Thus for panels (b), (c) and (d) Q_{po} was increased by a factor of 2, 3 and 4 respectively over its corresponding value of panel (a). The latter one was chosen in such a way as to make the system exhibit large period limit cycles. The period starts decreasing with increasing Q_{po} – as a matter of fact the period gets exactly to a half of its previous value as Q_{po} is increased by a factor of 2. This behaviour degenerates into a damped oscillation – steady state mode with increasing Q_{po} (panels c and d). This is exactly the behaviour we found in our analytical treatment – see Fig. 5. Therefore, despite the plethora of the physical processes introduced, the feedback loop still operates.

For low values of the magnetic field, ICS acts as a friction mechanism stabilizing the system and letting it reach quickly steady state. Fig. 17 shows an example where we ran the code for two cases. In the first, all processes were taken into account (dashed line), whereas in the second case, ICS was artificially switched-off (solid line). In the former case the system, after an initial peak, falls quickly into a steady state. In the latter it shows the limit cycle behaviour. The two cases are identical until the time when the compactness of soft photons becomes large and cannot be neglected any further in the electron cooling. This occurs around the time that the first peak in ℓ_γ appears, where the soft photon compactness becomes by a factor of $\sim 6 \times 10^3$ higher than the magnetic one. It is worth comparing the result shown in Fig. 17 with the one plotted in panel (a) of Fig. 15, where ICS was taken into account in an approximate way. In both cases the qualitative results are the same. If we use a higher value of the magnetic field for the example case shown in Fig. 17, we find that ICS alters the periodic behaviour only by decreasing the period. The temporal behaviour we find in this case, can be very well described by the corresponding one shown in panel (b) of Fig. 15. Suppression of ICS because of Klein-Nishina cutoff effects does not play an important role in this case, since we do not assume monoenergetic electron and photon distributions. Thus, most of the scatterings occur in the Thomson regime and Klein-Nishina cutoff effects are now small corrections. Finally, we note that the limit cycle behaviour of the system shown in Fig. 16 remains intact, although ICS was taken into account, since for the parameters used, the magnetic energy density is always larger than the soft photon one.

6 RELEVANCE TO ASTROPHYSICAL SOURCES

We turn next to examine the ideas presented in the previous sections in the context of possible applications of astrophysical interest. Whenever the system operates in the subcritical regime or the γ -rays are being absorbed mainly through the linear absorbing channel (see §4.1), our steady state spectra

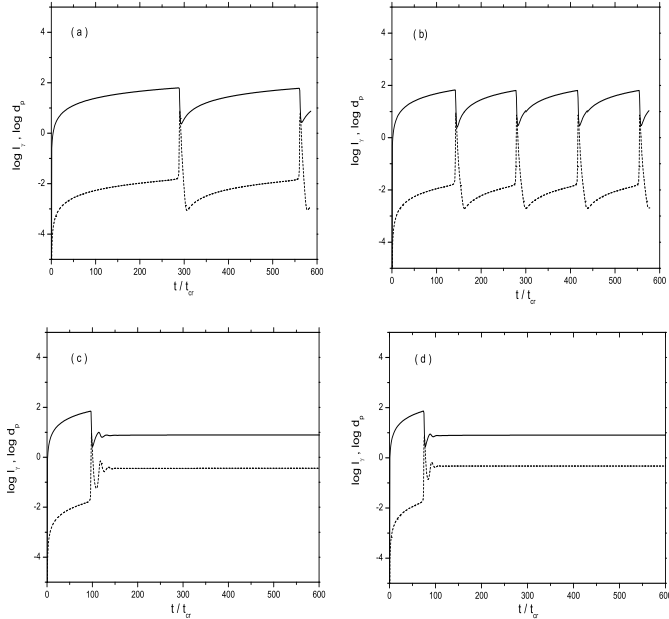


Figure 16. Time evolution of the system for four different proton injection rates or equivalently proton compactnesses, starting with $\ell_p^{\text{inj}} = 4.7 \times 10^{-5}$ in panel (a). In panels (b) to (d) ℓ_p^{inj} is increased over its previous value by an integer multiple of its initial value. The rest of the parameters used for this plot are: $B = 10$ G, $R = 10^{16}$ cm and $\gamma_p = 3 \times 10^7$. Solid and dashed lines show d_p and ℓ_γ respectively, where $d_p = \int d\gamma_p \gamma_p n_p(\gamma_p)$.

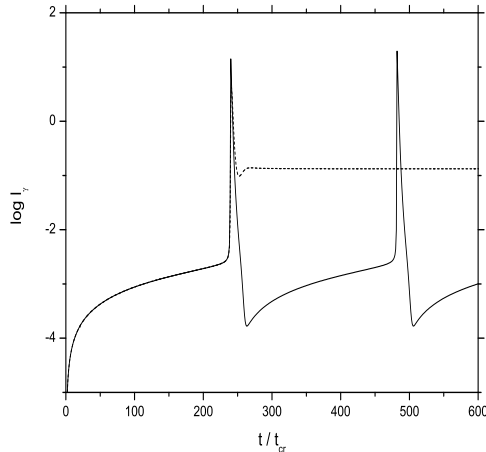


Figure 17. Photon compactness ℓ_γ as a function of time for two cases where, (i) inverse Compton scattering is taken into account (solid line) and (ii) it is artificially switched-off. The parameters used for this plot are: $B = 3.2$ G, $R = 10^{16}$ cm and $\gamma_p = 3 \times 10^7$, $\ell_p^{\text{inj}} = 7 \times 10^{-5}$.

are similar to those presented in the literature – for example see Böttcher (2007). On the other hand, if the system becomes supercritical and the absorption of γ -rays is strongly non-linear, then new possibilities open for astrophysical applications. These, according to §3 and §4, can be summarized in the following:

(i) All the components of the hadronic system exhibit an intrinsic variability with a well defined period, although the source is stationary.

(ii) The system reaches a steady state after going through a damping oscillatory phase. In this case a soft photon component emerges since a significant fraction of the energy stored in protons is transferred to lower energy photons via quenching of the γ -rays. At the same time the hard photon compactness reaches a limiting maximum value.

Both cases can, in principle, have relevance to astrophysical sources emitting in high energies, such as AGN. Time variability is a defining property of blazars and, in most cases, it shows a quite complex pattern (e.g., Mukherjee et al. 1999; Aharonian et al. 2007). We note that, even if the observations seem to contradict our results (see point (i) above), we have found that even small amplitude variations of the proton injection rate can lead to much more complicated time profiles than the ones presented so far. This is a promising topic. Therefore, a detailed study of the system towards this direction is required and is going to be the subject of a future work.

In the rest of this section we will focus on the second point. We will show specifically how we can apply our results in order to set an upper limit to parameter values used in the modelling of AGN multiwavelength spectra. This can be seen as an extension of the application presented in PM11.

The luminous blazar 3C 279 is a good example. A recent comprehensive review of observations can be found in Böttcher, Reimer, & Marscher (2009). Here we will mainly focus on the 2006 campaign, which discovered the source at VHE γ -rays, showing a high TeV flux (Albert et al. 2008), while the X-rays were at a much lower level.

Let us consider a spherical source of radius R moving with a Doppler factor δ with respect to us and containing a magnetic field of strength B . We further assume that ultra-relativistic protons with a power law distribution of index s are being constantly injected into the source with a rate given by

$$\tilde{Q}_p = \tilde{Q}_{p0} \gamma_p^{-s} H(\gamma_p - \gamma_{\min}) H(\gamma_{\max} - \gamma_p), \quad (45)$$

where γ_{\min} and γ_{\max} are the lower and upper limits of the injected distribution respectively. \tilde{Q}_{p0} is the normalization constant and is also directly related to the proton injection compactness as:

$$\ell_p^{\text{inj}} = \tilde{Q}_{p0} m_p c^2 \frac{\sigma_T R}{3t_{cr}} \frac{\gamma_{\min}^{-s+2} - \gamma_{\max}^{s+2}}{2-s} \quad (46)$$

or in terms of dimensionless quantities

$$\ell_p^{\text{inj}} = \frac{1}{3} Q_{p0} \frac{\gamma_{\min}^{-s+2} - \gamma_{\max}^{s+2}}{2-s}. \quad (47)$$

The transition of the system from the sub- to the supercritical regime can be better seen if initially there are no soft photons present in the source. For this, we try to fit only the

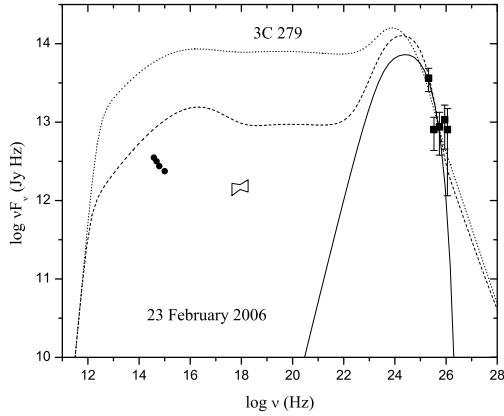


Figure 18. Multiwavelength spectra of 3C 279 obtained in the context of a pure hadronic model for $R = 3 \times 10^{16}$ cm, $B = 40$ G, $\delta = 20$, $\gamma_{\min} = 5 \times 10^8$, $\gamma_{\max} = 5 \times 10^9$, $s = 2.2$ and three proton injection compactnesses: $\ell_p^{\text{inj}} = 10^{-5}$ (solid line), 2×10^{-5} (dashed line) and 4×10^{-5} (dotted line). The symbols represent the observational data from February 2006.

TeV emission by considering a narrow power law proton energy distribution and no primary electron population. Thus, the multiwavelength spectrum is purely the result of proton primary and secondary emission.

Figure 18 shows the multiwavelength spectra obtained using the numerical code described in §5 for $R = 3 \times 10^{16}$ cm, $B = 40$ G, $\delta = 20$, $\gamma_{\min} = 5 \times 10^8$, $\gamma_{\max} = 5 \times 10^9$, $s = 2.2$ and for three values of the proton injection compactness starting with $\ell_p^{\text{inj}} = 10^{-5}$ (solid line) and increasing it over each previous value by a factor of two. For this set of parameters the produced γ -rays lie in the GeV-TeV regime. The spectrum for the lowest value of ℓ_p^{inj} (solid line) is obtained while the system is subcritical, and it is the only one that can give an acceptable fit of the TeV emission while at the same time does not violate the optical and X-ray observations. We see that an increase of ℓ_p^{inj} by just a factor of two drives the system into the supercritical regime. The onset of supercriticality is accompanied by the emergence of a soft emission component (dashed line), that becomes dominant for an even higher ℓ_p^{inj} (dotted line). The over-production of soft photons even in the second case is excluded directly by the observations, setting an upper limit to the proton injection compactness (for the specific example, $\ell_{p,\text{max}}^{\text{inj}} = 10^{-5}$).

If we were to use a lower value of δ to obtain the fit in the TeV energy range while keeping fixed the magnetic field strength, we would require a higher value of ℓ_p^{inj} , since $L_{\text{obs}} \propto \delta^4 L_{\text{int}}$, where L_{obs} and L_{int} are the luminosities in the observer's and in the comoving frame respectively. This choice of parameters would drive the system deep into the supercritical regime violating the optical and X-ray observations. PM11 have used similar arguments to set constraints on the Doppler factor δ by using an *ad-hoc* γ -ray injected luminosity. Here we go one step further since the injected γ -rays are related to a physical production mechanism. Thus, in this case we can set a limit on both δ and ℓ_p^{inj} . Moreover a potential flaring event observed only in the GeV part of the spectrum could not be fitted by just increasing the proton

injection luminosity, since this increase would affect also the optical and X-ray part of the spectrum, as the example of Fig. 18 suggests.

Thus, the effects of the underlying feedback mechanism can prove to be useful in setting lower limits to parameters, such as the Doppler factor δ . A systematic search of the parameter space is however out of the scope of the present paper.

7 DISCUSSION

Hadronic models have been extensively used for explaining AGN non-thermal emission while recently they have been applied, as well, to other compact objects. An interesting, but overlooked property of hadronic systems is their dynamical behaviour, which results from some underlying feedback mechanisms. In the present paper we have isolated and studied analytically one such loop that involves proton-photon pion production and photon quenching (SK07; PM11) of the produced γ -rays. Gamma-ray quenching results in automatic production of soft photons which then feed back producing more proton-photon cooling via pion production.

We have remarked that if protons are considered stationary in the source – an often made assumption, there are parameter space regimes which are characterized by an exponential growth of internally produced photons, making the system inherently unstable since the condition for proton stationarity is violated by the losses caused by the runaway photons – here the analogies to the ‘Compton catastrophe’ of leptonic plasmas are evident. The kinetic equation approach, which allows proton cooling to be explicitly taken into account, is suitable for studying in this case, the properties of the system. Protons, secondary electrons and photons, i.e., the main three components of the system, can be described by three coupled partial integro-differential equations. This ‘kinetic equation treatment’ has many advantages, as it is both energy conserving and time dependent.

In order to simplify the system of equations and make an analytical treatment possible we made a number of assumptions. As a first step we have retained only simplified expressions of the key processes by using δ -functions for the different particle distributions appearing in the problem. Furthermore, we used approximate expressions for the cross sections – see eqs. (7) and (35). However, one of the major simplifying assumptions we made was the elimination of the electron kinetic equation from the system of eqs. (15). The rationale for this is that the electron cooling timescale, for typical values of the magnetic field and electron Lorentz factors, is much smaller than the crossing time of the source. Thus, electron cooling is considered to be instantaneous.

Ignoring absorption of the hard photons on the external ones, we have found that an increase of the proton injection rate leads to an analogous increase of the proton density and of the hard photon luminosity resulting from photopion. If the latter does not get to a high value as to trigger quenching, the system is linear and reaches a steady state. If, however, the combination of the initial parameters is such that leads the hard photons past the quenching threshold, then the latter are automatically absorbed and the soft photons which are spontaneously produced serve as targets for extra proton cooling. In this case we have shown analytically by

performing an eigenvector/eigenvalue analysis, that for hard photon densities close but above critical the system goes through a limit cycle behaviour of the prey-predator type. For even higher hard photon densities, the system reaches a steady state which is achieved after protons and photons exhibit a series of damped oscillations. This steady state occurs at very different values from the ones achieved while the system is subcritical and this discontinuity is another indication of the system's supercriticality. It is interesting to note that duty-cycle behaviour in hadronic systems was reported by Stern & Svensson (1991) using a Monte Carlo code and by MPK05 using a kinetic equation approach. However both papers were numerical and the authors, while giving ample physical reasoning for the behaviour, fell short of presenting a mathematical proof. Here for the first time we present such an interpretation and show beyond doubt, that hadronic systems can indeed exhibit the aforementioned behaviour.

As a next step we have shown semi-analytically that when absorption of the produced hard photons on the external ones is included, then the behaviour of the system depends also on the corresponding optical depth. If this takes low values, then the system behaves as described above since the non-linear processes continue to play a dominant role in the dynamics of the system. If, on the other hand, the optical depth takes high values, the systematic depletion of hard photons tends to stabilize the system which reaches a steady state after it goes through a damped oscillation mode, i.e., no limit cycle behaviour was found in this case. It is interesting however to note that, even in this case, the hard photons cannot reach a steady state above the critical value of quenching. This can only mean that quenching remains a fundamental intrinsic property of the system.

Furthermore, if we are to add more physical processes to the system, these tend to stabilize it as they redistribute part of the radiated energy away from the operating feedback loops. For example, inverse Compton scattering can act as a competing energy loss mechanism for electrons to synchrotron radiation. If it dominates, then the system changes behaviour moving faster to a steady state. However for strong enough B-fields, we found that the system retains the analytically derived properties.

The above results, were also verified by using a numerical code where the full expressions for the emissivities of the various radiative processes and for the various relevant cross sections were used. While the details change from our simplified analytical approach, we were able to confirm qualitatively our analytical results which predict the transition from the subcritical linear regime to the supercritical oscillatory one with increasing proton density. In addition, we were able to verify the role of other processes, like inverse Compton scattering, which we had taken in our analytical treatment only approximately into account. We note that the qualitative analogies between the results of the two treatments justify also *a posteriori* and in an independent way the validity of our simplifying assumptions.

Our results indicate that higher proton injection rates tend to push the system into the non-linear regime with the external photons acting more as catalysts; on the other hand, higher external photon densities act on the opposite direction and tend to linearize the system. Preliminary numerical calculations (Dimitrakoudis et al. – in preparation) show that this trend remains, if one is to replace the δ -

function distributions used in the present treatment with the more astrophysically relevant power-laws.

Finally, as an example of astrophysical interest, we have used the numerical code described in §5, which can treat self-consistently both the non-linear development of EM cascades and proton cooling, in order to make a fit to the TeV emission of blazar 3C 279. We have shown that acceptable fits can be obtained only for high values of the Doppler factor ($\delta \gtrsim 20$), given that typical values for the magnetic field in the context of hadronic models are considered ($B \simeq 10 - 60$ G). However, this is only an indicative example of the potential applications of the model. Obviously one needs to thoroughly study the parameter space before providing exact fitting values. Another potential direction is the study of the inherent variability signatures of the system in cases where the source itself is variable.

The supercriticality related to the feedback mechanism studied in the present paper is by no means the only one that can occur in hadronic systems. If one was to replace the photopion interactions by another production mechanism of γ -rays, e.g., proton synchrotron radiation, and study the same feedback loop outlined in §1, one would again find that the system enters a supercritical regime. However, the parameter values that would enable the transition from the subcritical to the supercritical regime, as well as the details concerning the transition itself, would differ from those shown in the present work, due to different cross sections, emissivities and energy threshold criteria. Furthermore, we cannot exclude that even other loops operate as well in a hadronic system – see Kirk & Mastichiadis (1992), Dimitrakoudis et al. (to appear in 2012). Actually, more than one of the different feedback mechanisms can operate simultaneously in a 'real' hadronic system. Because of this, a comprehensive search of its parameter space demands the use of the numerical code described in §5 and it is going to be the subject of a future work. At any rate, we have shown that hadronic models constitute one more example in the growing list of dynamical systems and as such they need to be further investigated.

ACKNOWLEDGMENTS

We would like to thank Drs. R. J. Protheroe and A. Reimer for making available the SOPHIA results to us and S. Dimitrakoudis for incorporating them in the numerical code. We would like to thank also Drs. N. Vlahakis and C. Efthymiopoulos for useful comments and discussions. This research has been co-financed by the European Union (European Social Fund - ESF) and Greek national funds through the Operational Program 'Education and Lifelong Learning' of the National Strategic Reference Framework (NSRF) - Research Funding Program: Heracleitus II. Investing in knowledge society through the European Social Fund.

APPENDIX A: STABILITY ANALYSIS OF THE TRIVIAL STATIONARY SOLUTION

Consider the system (S)

$$\dot{x} = -x + An_{\text{ex}}z + Azy - C_{\text{h}}yx \quad (\text{A1})$$

$$\dot{y} = -y + C_s y x \quad (\text{A2})$$

$$\dot{z} = Q_{\text{po}} - \frac{z}{\tau_p} - \sigma_{\text{p}\gamma}^0 n_{\text{ex}} z - \sigma_{\text{p}\gamma}^0 z y \quad (\text{A3})$$

where variables (x, y, z) stand for $(n_{\text{h}}, n_{\text{s}}, n_{\text{p}})$. The fixed points of the system, $P_i(x_0^{(i)}, y_0^{(i)}, z_0^{(i)})$ with $i = 1, 2, 3$ can be found by setting $\dot{x} = \dot{y} = \dot{z} = 0$. The first fixed point is nothing more than the trivial steady state solution of the system in the case of no quenching:

$$x_0^{(1)} = A n_{\text{ex}} \frac{Q_{\text{po}}}{G_{\text{p}}} \quad (\text{A4})$$

$$y_0^{(1)} = 0 \quad (\text{A5})$$

$$z_0^{(1)} = \frac{Q_{\text{po}}}{G_{\text{p}}}. \quad (\text{A6})$$

The remaining fixed points have $x_0^{(2),(3)} = 1/C_s$ and $z_0^{(2),(3)} = \frac{Q_{\text{po}}}{G_{\text{p}} + \sigma_{\text{p}\gamma}^0 y_0^{(2),(3)}}$, where $y_0^{(2),(3)}$ are the real roots of the equation

$$y^2 + y \left(\frac{G_{\text{p}}}{\sigma_{\text{p}\gamma}^0} + \frac{1}{C_{\text{h}}} - \frac{Q_{\text{po}} A C_s}{\sigma_{\text{p}\gamma}^0 C_{\text{h}}} \right) + \frac{G_{\text{p}} - Q_{\text{po}} A n_{\text{ex}} C_s}{\sigma_{\text{p}\gamma}^0 C_{\text{h}}} = 0. \quad (\text{A7})$$

We make the convention that $y_0^{(2)}$ is the positive real root that has physical meaning. It is interesting to examine the behaviour of the system when it is slightly perturbed by its steady state, i.e., $x = x_0^{(1)} + x', y = y', z = z_0^{(1)} + z'$. For this we linearize system (S) with respect to the perturbed quantities:

$$\dot{x}' = -x' + (A z_0^{(1)} - C_{\text{h}} x_0^{(1)}) y' + A n_{\text{ex}} z' \quad (\text{A8})$$

$$\dot{y}' = (-1 + C_s x_0^{(1)}) y' \quad (\text{A9})$$

$$\dot{z}' = -\sigma_{\text{p}\gamma}^0 z_0^{(1)} y' - G_{\text{p}} z'. \quad (\text{A10})$$

For the second equation that is not coupled to the other two we find an exponential growth or decay $y'(\tau) = y'(0)e^{s\tau}$ depending on the sign of $s = -1 + C_s x_0^{(1)}$. First suppose that $s < 0$. $y' \rightarrow 0$ holds for $\tau \gtrsim 1/s$ and the three linearized equations degenerate to two. The matrix of the two dimensional system is

$$M_1 = \begin{pmatrix} -1 & A n_{\text{ex}} \\ 0 & -G_{\text{p}} \end{pmatrix}$$

with determinant $\Delta(M_1) = G_{\text{p}} > 0$ and trace $\text{Tr}(M_1) = -1 - G_{\text{p}} < 0$. Thus, in this case the point P_1 is stable. This simple analysis does not apply in the case of $s > 0$. However, it can be easily shown that both z' and x' are $\propto e^{s\tau}$ for large enough times. Thus, in this case all the perturbed quantities grow with time and P_1 can be characterized as unstable.

APPENDIX B: STABILITY ANALYSIS OF THE NON-TRIVIAL STATIONARY SOLUTION

In general, the topology of a vector field near its fixed points can be studied through the Jacobian matrix of the vector field at the corresponding points. Specifically, the classification of fixed points in different types is made by an eigenvalue/eigenvector analysis of the Jacobian matrix. This analysis is widely used for two-dimensional vector fields, leading to a few types of fixed points. This is not the case for three dimensional systems, where the classification of the fixed points in types is more complicated. In our work we

have adopted the classification presented in Theisel et al. (2003).

Here we apply the eigenvalue analysis to the three dimensional vector field $\mathbf{v} = (\dot{n}_{\text{h}}, \dot{n}_{\text{s}}, \dot{n}_{\text{p}})^T$. We consider the second non-trivial stationary solution of the system S2. Thus, the set of equations (S2) after linearization at the point P_2 can be written in the form

$$\begin{pmatrix} \dot{n}_{\text{h}} \\ \dot{n}_{\text{s}} \\ \dot{n}_{\text{p}} \end{pmatrix} = M_2 \begin{pmatrix} n_{\text{h}} \\ n_{\text{s}} \\ n_{\text{p}} \end{pmatrix}$$

where the matrix M_2 is given by

$$M_2 = \begin{pmatrix} -1 - C_{\text{h}} y_0^{(2)} & A z_0^{(2)} - C_{\text{h}} x_0^{(2)} & A(n_{\text{ex}} + y_0^{(2)}) \\ C_s y_0^{(2)} & 0 & 0 \\ 0 & -\sigma_{\text{p}\gamma}^0 z_0^{(2)} & -(G_{\text{p}} + \sigma_{\text{p}\gamma}^0 y_0^{(2)}) \end{pmatrix}.$$

The eigenvalues are the roots of its characteristic polynomial

$$P(\lambda) = \lambda^3 + a_1 \lambda^2 + a_2 \lambda + a_3, \quad (\text{B1})$$

where

$$a_1 = -\text{Tr}(M_2) \quad (\text{B2})$$

$$a_2 = \left(1 + C_{\text{h}} y_0^{(2)} \right) \left(G_{\text{p}} + \sigma_{\text{p}\gamma}^0 y_0^{(2)} \right) - C_s y_0^{(2)} \left(A z_0^{(2)} - C_{\text{h}} / C_s \right) \quad (\text{B3})$$

$$a_3 = C_s y_0^{(2)} \left[A \sigma_{\text{p}\gamma}^0 z_0^{(2)} \left(n_{\text{ex}} + y_0^{(2)} \right) - \left(A z_0^{(2)} - C_{\text{h}} / C_s \right) \left(G_{\text{p}} + \sigma_{\text{p}\gamma}^0 y_0^{(2)} \right) \right]. \quad (\text{B4})$$

The number of real and complex roots of the equation $P(\lambda) = 0$ can be determined, if one knows the signs of the constants. For values relevant to our physical problem, one finds that (i) either all three constants are positive or (ii) only a_2 is negative. In the first case the polynomial has 3 negative real roots or 1 negative real root and two complex conjugates, while in the second case there is always 1 negative real root and 2 complex conjugates with positive real parts.

Figure B1 shows the dependence of constants a_i on Q_{po} and n_{ex} . Since a logarithmic scale is used, the negative values of a_2 are not shown.

APPENDIX C: DERIVATION OF THE CRITICAL γ -RAY COMPACTNESS

Let us assume that hard photons are being injected into a spherical source with a constant rate $Q_{\text{h}}^{\text{inj}}$ that corresponds to a compactness $\ell_{\text{h}}^{\text{inj}}$ and that no soft photons are initially present in the source. Automatic quenching of hard photons is possible if the injected compactness exceeds a certain value. In this case, electron-positron pairs are being created spontaneously in the source, emitting synchrotron radiation. Hard photons then undergo further absorption on the aforementioned soft photons and a non-linear loop of processes begins to operate. The equations that describe the above physical system can be written in the following form:

$$\dot{n}_{\text{h}} = Q_{\text{h}}^{\text{inj}} - n_{\text{h}} - C_{\text{h}} n_{\text{s}} n_{\text{h}} \quad (\text{C1})$$

$$\dot{n}_{\text{s}} = -n_{\text{s}} + C_s n_{\text{s}} n_{\text{h}}, \quad (\text{C2})$$

where the constants C_{h} and C_s are defined in eq. (33).

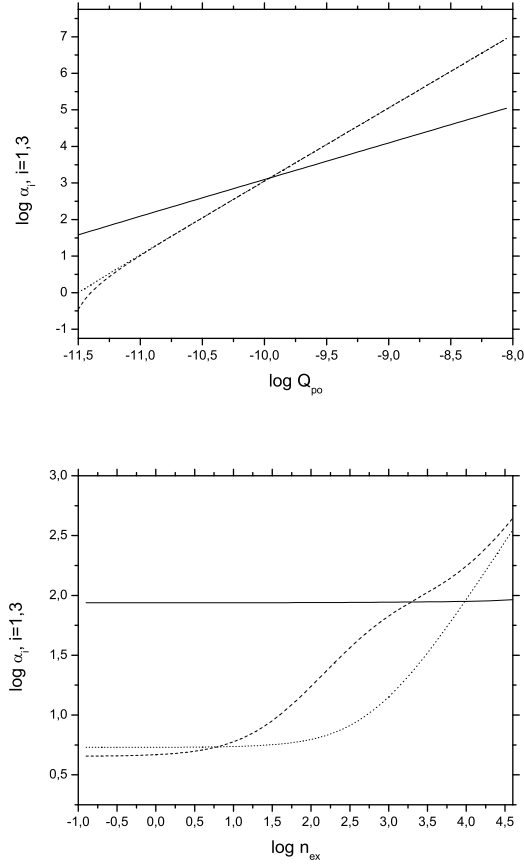


Figure B1. Dependence of the constants of the characteristic polynomial $P(\lambda)$ on Q_{po} for $n_{ex} = 2$ (top panel) and on n_{ex} for $\log Q_{po} = -11.15$ (bottom panel), for a range of values relevant to the physical problem. In both panels solid, dashed and dotted lines represent the constants a_1 , a_2 and a_3 respectively.

There is a trivial stationary solution of the system (C2): $\bar{n}_h = Q_h^{inj}$, $\bar{n}_s = 0$, that corresponds to the free propagation of hard photons through the source, where pairs and soft photons are absent. The Jacobian matrix evaluated for this solution has two real eigenvalues. For $Q_h^{inj} < 1/C_s$ both are negative. Thus, the solution is stable. Moreover, in this case the system has no other physically acceptable solution, i.e., $n_s > 0$. However, if $Q_h^{inj} > 1/C_s$ one of the eigenvalues becomes positive and the solution with a zero soft photon population becomes unstable. Even a perturbation in the initially absent soft photon distribution is sufficient for its subsequent growth. In this region, a second stationary solution of the system (C2) appears. This is $\bar{n}_h = 1/C_s$, $\bar{n}_s = (Q_h^{inj} - \bar{n}_h)/C_h \bar{n}_h$ and one can show that for this region both eigenvalues of the corresponding Jacobian matrix are negative, i.e., the solution is stable.

Summarizing, the critical injection rate is $1/C_s$, which can be transformed to the critical compactness:

$$\ell_h^{cr} = \frac{\epsilon_h}{3C_s}. \quad (C3)$$

REFERENCES

- Aharonian F. et al., 2007, *ApJ*, 664, L71
Asano K., Inoue S., 2007, *ApJ*, 671, 645
Asano K., Inoue S., Mészáros P., 2009, *ApJ*, 699, 953
Begelman M. C., Rudak B., Sikora M., 1990, *ApJ*, 362, 38
Böttcher M., 2007, *Ap&SS*, 309, 95
Böttcher M., 2010, *ArXiv e-prints*
Böttcher M., Dermer C. D., 1998, *ApJ*, 499, L131
Böttcher M., Reimer A., Marscher A. P., 2009, *ApJ*, 703, 1168
Coppi P. S., Blandford R. D., 1990, *MNRAS*, 245, 453
Dimitrakoudis et al., to appear in 2012, *IJMPC (International Journal of Modern Physics C)*
Kazanas D., Ellison D. C., 1986, *ApJ*, 304, 178
Kazanas D., Georganopoulos M., Mastichiadis A., 2002, *ApJ*, 578, L15
Kirk J. G., Mastichiadis A., 1992, *Nature*, 360, 135
Mannheim K., 1993, *A&A*, 269, 67
Mastichiadis A., Kazanas D., 2006, *ApJ*, 645, 416
Mastichiadis A., Kazanas D., 2009, *ApJ*, 694, L54
Mastichiadis A., Kirk J. G., 1995, *A&A*, 295, 613
Mastichiadis A., Protheroe R. J., Kirk J. G., 2005, *A&A*, 433, 765
Moderski R., Sikora M., Coppi P. S., Aharonian F., 2005, *MNRAS*, 363, 954
Mücke A., Engel R., Rachen J. P., Protheroe R. J., Stanev T., 2000, *Computer Physics Communications*, 124, 290
Mücke A., Protheroe R. J., 2001, *Astroparticle Physics*, 15, 121
Mukherjee R. et al., 1999, *ApJ*, 527, 132
Paredes J. M., Bosch-Ramon V., Romero G. E., 2005, in *American Institute of Physics Conference Series*, Vol. 801, *Astrophysical Sources of High Energy Particles and Radiation*, T. Bulik, B. Rudak, & G. Madejski, ed., pp. 224–226
Petropoulou M., Mastichiadis A., 2011, *A&A*, 532, A11+
Romero G. E., Christiansen H. R., Orellana M., 2005, *ApJ*, 632, 1093
Romero G. E., Torres D. F., Kaufman Bernadó M. M., Mirabel I. F., 2003, *A&A*, 410, L1
Sikora M., Kirk J. G., Begelman M. C., Schneider P., 1987, *ApJ*, 320, L81
Stawarz L., Kirk J. G., 2007, *ApJ*, 661, L17
Stern B., Svensson R., 1991, in *Lecture Notes in Physics*, Berlin Springer Verlag, Vol. 391, *Relativistic Hadrons in Cosmic Compact Objects*, A. A. Zdziarski & M. Sikora, ed., pp. 41–+
Stern B. E., Begelman M. C., Sikora M., Svensson R., 1995, *MNRAS*, 272, 291
Stern B. E., Sikora M., Svensson R., 1992, in *American Institute of Physics Conference Series*, Vol. 254, *American Institute of Physics Conference Series*, S. S. Holt, S. G. Neff, & C. M. Urry, ed., pp. 313–316
Theisel H., Weinkauff T., Hege H.-C., Seidel H.-P., 2003, in *Proc. IEEE Visualization 2003*, Turk G., van Wijk J. J., Moorhead R., eds., Seattle, U.S.A., pp. 225–232